New constraints on late Holocene eustatic sea-level changes from Mahé, Seychelles

Sarah A. Woodroffe*[1], Antony J. Long[1], Glenn A. Milne[2], Charlotte Bryant[3], Alexander Thomas[4]

[1] Department of Geography, Durham University, Lower Mountjoy, South Road, Durham, DH1 3LE, UK. s.a.woodroffe@durham.ac.uk 0044 191 334 1932.

[2] Department of Earth Sciences, University of Ottawa, FSS Hall, Ottawa, K1N 6N5, Canada.

[3] NERC Radiocarbon Facility (East Kilbride), Scottish Enterprise Technology Park, Rankine Avenue, East Kilbride, Glasgow, G75 0QF, UK.

[4] Department of Geosciences, University of Edinburgh, Grant Institute, The King's Buildings, West Mains Road, Edinburgh EH9 3JW, UK.

*corresponding author

Abstract

This study provides new estimates of globally integrated ice sheet melt during the late Holocene (since 4 ka BP) from Seychelles in the western Indian Ocean, a tectonically stable, far field location where the necessary Glacial-Isostatic Adjustment (GIA) correction is small and is relatively insensitive to predictions using different Earth viscosity profiles. We compare sea-level data from Seychelles to estimates of eustasy from two GIA models, ICE-5G and EUST3, which represent end-members in the quantity of global melt during the late Holocene. We use data from a range of coastal environments including fringing reef, present day beaches, fossil plateau and mangrove deposits on the largest island of the Seychelles archipelago, Mahé to reconstruct relative sea-level changes. Our data suggest that extensive coastal deposits of carbonate-rich sands that fringe the west coast formed in the last 2 ka and the horizontal nature of their surface topography suggests RSL stability during this period. Mangrove sediments preserved behind these deposits and in river mouths date to c. 2-1.5 ka and indicate that RSL was between -2 m and present during this interval. Correcting the reconstructed sea level data using a suite of optimal GIA models based on the two ice models mentioned above and a large number (c. 350) of Earth viscosity models gives a result that is consistent with the sedimentological constraints. When uncertainties in both model results and data are considered, it is possible to rule out eustatic sea levels below c. 2 m and more than a few decimetres above present during the past two millennia. This uncertainty is dominated by error in the reconstructions rather than the model predictions. We note, however, that our estimates of eustasy are more compatible with the EUST3 model compared to the ICE-5G model during the late Holocene (2-1 ka BP. Our evidence from Seychelles shows that the timing of when eustatic sea level first rose close to present is between the predictions of the two end-member GIA models presented here (4 ka BP for ICE-5G and 1 ka BP for EUST3). Using all lines of evidence currently available from Mahé we suggest that the eustatic contribution during the last 2 ka has been less than 2 m. This conclusion is drawn from a

tectonically stable, far-field region that is relatively insensitive to earth and ice model uncertainties, and implies that global eustasy has been relatively insensitive to climate fluctuations over the pre-industrial part of the last 2 ka.

Keywords: Eustasy, relative sea-level, mangroves, Seychelles, late Holocene; glacial-isostatic adjustment.

1. Introduction

Relative sea-level (RSL) changes around the world since the Last Glacial Maximum (LGM) reflect the interaction of ice sheets, oceans and the solid earth. In locations far from the centres of former ice masses (far-field locations), the influx of glacial meltwater into the oceans dominates RSL and so reconstructions from such sites are commonly used to constrain volumetric changes in global grounded ice through time (Fleming et al. 1998; Yokoyama et al. 2000; Lambeck 2002; Peltier 2002; Milne et al. 2005; Peltier and Fairbanks 2006; Bradley et al. 2011; Deschamps et al. 2012; Lambeck et al. 2014). Most far-field records of RSL from the LGM sea-level lowstand to present used by geophysical models are coral-based (Chappell and Polach 1991; Bard et al. 1996; Peltier and Fairbanks 2006), with a smaller number of sediment-based archives that focus on the LGM minimum (e.g. Hanebuth et al. 2000; Yokoyama et al. 2000). None of these records provide any observations and hence model constraints during the late Holocene. More recent studies by Bradley et al. (2011) and Lambeck et al. (2014) have tried to redress this focus on long, coral-based records by including evidence from coral and sediment-based archives in the mid to late Holocene.

Though many studies claim to record "eustatic" changes, i.e. the global mean change associated with meltwater addition only (e.g. Whitehouse and Bradley 2013), there is in fact no single location on earth where we can directly measure eustasy through time. Even in far-field locations, isostatic, gravitational and rotational effects associated with Glacial-Isostatic Adjustment (GIA) can have a significant influence on regional RSL changes (Clark et al. 1978; Milne and Mitrovica 2008; Lambeck et al. 2014). In addition to these regional changes, the globally uniform signal known as ocean syphoning (Mitrovica and Peltier 1991; Mitrovica and Milne 2002) also has a significant effect. These factors are less apparent during the deglacial and early Holocene periods because of rapid sea-level rise due to ice sheet melt. However during the mid- to late-Holocene when the rate of ice melt was reduced or eliminated, these ongoing GIA processes become more evident and can dominate the observed far-field RSL signal, leading to high stands or continued RSL rise. Of course, other processes such as tectonics can cause local RSL to deviate significantly from eustasy.

1.1 Mid to late-Holocene grounded ice melt

Several geophysical models suggest that global ice melt ceased in the mid Holocene. Milne et al. (2005) suggest that RSL data from the Caribbean and South America are compatible with no significant net melt (i.e. >1 m eustatic equivalent) of grounded ice since 6 ka BP. Peltier (2002) shows that RSL predictions for equatorial Pacific locations using the ICE-4G model do not match coral-based reconstructions of a mid-Holocene highstand if global ice melt (at 0.25 or 0.5 mm/yr from Antarctica or Greenland) continues after 4 ka BP (thousand years before present), although they predict more than 2 m of global ice melt between 6-4 ka BP. However modelling studies that consider other mid- to late-Holocene RSL data from intermediate and far-field locations infer that some ice melt continued until more recently (Nakada and Lambeck 1989; Lambeck 2002; Lambeck and Purcell 2005; Bradley et al. 2011; Lambeck et al. 2014). For example, the global ice model in Bradley et al. (2011), constrained using RSL data from China and the Malay-Thai Peninsula, includes approximately 1.5 m of grounded ice melt between 4-1 ka BP, and Lambeck et al. (2014) suggest a total contribution of up to 1 m in the past 4.2 ka constrained using a large suite of RSL data from across the far-field. The eustatic functions of the EUST3 (Bradley et al., 2011) and ICE-5G (Peltier, 2002) ice models therefore represent end members in the quantity of melt during the mid-to-late Holocene. Determining which is the more accurate is an important task towards producing improved GIA models and a better understanding of polar ice sheet response to climate during this period.

Despite different estimates of the magnitude and timing of any continued ice melt in the mid- to late-Holocene, most modelling studies agree that major melt finished during the mid-Holocene. The Laurentide Ice Sheet had largely disappeared by 6.8 ka BP, with small ice caps in northern Canada contributing only a minor quantity to global sea-level until c. 5.5 ka BP (Carlson et al. 2008). In Greenland, parts of the western and southern sectors of the ice sheet reached their minimum extent in the mid-Holocene before re-growing in the late Holocene during the cool neoglacial period (Kelly 1980; Simpson et al. 2009). Small ice caps and alpine glaciers in the northern and southern hemispheres also grew during the neoglacial (e.g. Patagonia, Alaska, western USA; Konrad and Clark 1998; Glasser et al. 2004; Glasser et al. 2005; Barclay et al. 2009), and together these ice masses potentially caused a small (decimetre-scale) draw-down in global sea level. This leaves Antarctica as the main potential source of late Holocene eustasy (Nakada and Lambeck 1988). A study of glacial retreat across the Ross Sea embayment in Antarctica suggests the ice shelf passed a grounding line c. 250 km beyond its present position only 3.2 ka BP (Conway et al. 1999) and there is evidence that ice in the Marie Byrd region of west Antarctica has melted steadily through the Holocene into recent times (Stone et al. 2003). However a general paucity of field observations on ice margin change during the late Holocene means debates remain about the potential contribution of Antarctica to any late Holocene eustatic sea-level rise (Whitehouse et al. 2012). The outstanding question is, therefore: has there been significant (>1 m global sea-level equivalent) ice melt during the mid- to late-Holocene (since c. 5 ka BP), and if so when did it occur, at what rate of change and from which source(s)?

2.RSL and eustasy in the far-field

In theory, RSL data from anywhere in the world can be used to constrain global grounded ice volume once the non-eustatic contributing factors are isolated. However, isolating these factors is a non-trivial exercise because uncertainties in GIA models are not uniform over time or space. For example, some sites are more or less sensitive to model assumptions regarding earth rheology and ice model parameters. Therefore, a sensible approach to this problem is to generate RSL data from sites where the non-eustatic (GIA) components tend to cancel (i.e. departures from eustasy are small) and where the sensitivity of the non-eustatic signal to uncertainties in the parameters of the GIA model are small.

Seychelles is in one of the few regions of the world where RSL is modelled to be within 1 m of eustasy during the last 6 ka, and where the GIA correction is relatively insensitive to predictions using different Earth viscosity profiles (Milne and Mitrovica, 2008). It is also a tectonically stable region (Israelson and Wohlfarth 1999). Previous Holocene studies here rely primarily on cored coral from coastal reefs, which provide relatively imprecise constraints on RSL during the early and mid-Holocene but very little late data as RSL reached close to present. The region supports a range of mangrove environments and extensive beach sand deposits that provide potential alternative sources of RSL data. In this study we combine data from these different sources to reconstruct past sea-level changes and coastal evolution in Seychelles. We use our estimates of late-Holocene RSL to estimate eustatic changes using two global ice models - ICE-5G (Peltier 2004) and EUST3 (Bradley et al., 2011) – and a large suite of Earth viscosity models. These two ice models were adopted as they include contrasting end-member estimates of ice volume changes during the late Holocene (see above) and so represent a conservative estimate of model uncertainty in this regard. We conclude that RSL in Seychelles had risen to within c. 2 m of present by 2 ka BP, and has been within c. -1 m of present since 1 ka BP. This estimate is then considered in the context of better constraining the eustatic function during the late Holocene, to address the question highlighted above and to test which current ice sheet volume estimates are most accurate.

2.1 Field location

Seychelles is an archipelago of 115 islands, spread across the southwestern Indian Ocean between 56° 14’ and 46° 23’ E and 3° 43’ and 10° 13’ S (Figure 1). The main granitic islands, which are thought to be tectonically stable over Quaternary timescales (Israelson and Wohlfarth 1999), lie in the northeast of the archipelago, with the largest and principal island of Mahé at 4° 41’S, 55° 28’E. The geology of these northern islands is Precambrian granite with dolerite intrusions; they sit on the Seychelles Bank, a 43,000 km^3 area of shallow shelf between 44-65 m deep, once part of a micro-continent connected to India and

Madagascar (Braithwaite et al. 2000; Torsvik et al. 2001). Mahé sits at the centre of the Seychelles Bank, with a 50-100 km-wide shallow shelf surrounding the island (Figure 1A). The island is largely mountainous (up to 905 m asl) with a narrow coastal strip dominated by headlands, bays and river mouths that are surrounded by extant and reclaimed mangroves and fringing reefs. Reefs are better developed on the east than the west coast where they are protected from the impact of waves generated by the NW monsoon (October – March). Bays around the island are partly filled by the 'plateau'; a discontinuous belt of carbonate sands up to 500 m wide that borders the present beach and reef flat and which has a surface relief that is up to a metre above highest tide level (Lewis 1969; Braithwaite et al. 2000). We hypothesise that these sands are fossil beach features which formed on the fringing reef flat when Holocene RSL was close to or above present. In some locations the sands form a coastal barrier behind which mangroves had developed, many of which are now reclaimed. The age and mode of formation of the plateau have not been previously investigated in detail. The present tidal range at Port Victoria on Mahé is 2.1 m, with MHWST and HAT 0.55 m and 1.05 m above MTL respectively (Admiralty Tide Tables 2009).

2.2 Previous studies into late Holocene RSL in Seychelles

Dated cores taken from a fringing coral reef at Anse aux Pins on Mahé (Figure 1) extend back to c. 10 ka BP (Braithwaite et al. 2000; Camoin et al. 2004). These authors interpret this reef to have been in "catch-up" mode through the Holocene, with a variable relationship between coral and water depth (Camoin et al. 2004). The youngest dated sample of coral is 1.8 m below the modern reef surface and dated to c. 3.7 ka BP, which is interpreted as evidence for local late Holocene RSL and reef stabilisation. The reef cores consist primarily of storm-derived coral, unconsolidated sands and skeletal debris, and therefore their use as precise RSL indicators is problematic. Despite this difficulty, Camoin et al. (2004) combine radiocarbon dated samples from Anse aux Pins with cored coral records from other SW Indian Ocean islands to reconstruct Holocene RSL changes in the region. They suggest that RSL first reached present c. 3-2.5 ka BP , inferring that any time lag between RSL reaching present and reef stabilisation was very small.

Evidence for a late Holocene RSL highstand in Seychelles is scarce, although Pirazzoli et al. (1990) report raised 1 ka old coral-rich conglomerates on St. Joseph and Farqhar atolls (Figure 1) which they suggest formed during a storm or tsunami, but were then lithified when RSL was c. 0.8 – 1.2 m above present. Camoin et al. (2004) attribute the apparent lack of Holocene RSL highstands on islands in the SW Indian Ocean to hydro-isostatic sea floor subsidence after the end of global ice melt.

3.Methods

3.1 RSL reconstruction

This study focuses on three sites on the west coast of Mahé; Barbarons and Anse Boileau, where river-mouth mangrove, fringing reef, beach and plateau deposits occur, and Anse a la Mouche, where only reef, beach and plateau deposits are found (Figure 1). We cored and surveyed the coastal geomorphology at each site, from the present day fringing reef flat, over the present day beach crest and plateau deposits into riverine mangroves where these were present. These mangrove environments often occur landward of the plateau in protected estuarine environments. We took cores through plateau sands with a hand-operated gouge corer and used a Russian-type corer in the mangroves. We collected undisturbed sample cores from the mangroves to return to the laboratory for further analysis, which were stored at 4 °C. We levelled the modern beaches and plateau deposits using a level and staff, relating measurements to mean tide level (MTL) by taking timed water level measurements in quiet water locations (within river mouths to minimise error) and correcting to simultaneous readings from the Port Victoria tide gauge on Mahé (estimated accuracy ± 0.05 m). The error in estimating elevation was incorporated in the total RSL reconstruction error by summing the different squared errors and square-rooting the total (root-squared error). We also collected selected fragments of reworked coral from cores within the plateau for AMS ^{14}C and U-Th dating, which provide maximum ages for their deposition.

To attempt quantitative RSL reconstructions from the mangrove sediments, we sampled the top 1 cm of mangrove at 47 locations across the River Dauban mangrove at <5 cm vertical intervals, with the intent to develop a training set of modern microfossil assemblages (diatoms and foraminifera) to understand their vertical distribution across the mangrove environment (see for example, Woodroffe et al. 2005). However foraminifera were not present in the surface or fossil sediments, and diatoms, although present at the surface, were not found in any of the core sediments below the top few cm.

The present day ecology of the mangroves on the west coast of Mahé is typified by an upper mangrove between broadly mean high water of spring and neap tide (MHWST and MHWNT, respectively) which is dominated by *Avicennia marina*, *Bruguiera gymnorrhiza* and *Xylocarpus granatum*, which is replaced by *Rhizophora mucronata*, *Sonneratia alba* and *Avicennia marina* at lower elevations, close to MTL. There are areas of hypersaline bare-ground between MHWST and highest astronomical tide (HAT) that comprise coarse sand or mud and may support localised communities of *Nypa fruticans* and *Acrostrichum aureum* below a terrestrial habitat dominated by *Pandanas* and *Cocos nucifera*. We surveyed the upper and lower limit of mangrove vegetation at 20 different locations at Barbarons and Anse Boileau. The median value for the upper and lower limit of mangrove vegetation was at +0.8 m ± 0.1 m and -0.39 m ± 0.22 m MTL, respectively. This range gives an indicative meaning for mangrove sediments of +0.2 m MTL ± 0.6 m, which represents more than half of the tidal range on Mahé (2.1 m). This uncertainty is larger than we had hoped

to achieve, but reflects the non-preservation of alternative microfossil proxies (e.g. diatoms or foraminifera). Loss on Ignition and % carbonate values from surface sediments within the present day mangrove provide no additional indication of elevation within the tidal range because values fluctuate throughout the mangrove environment. In other tropical locations, where mangroves are extensive and vegetation zonation is better developed, others have successfully reconstructed RSL utilising pollen found within surface and fossil mangrove deposits (e.g. Engelhart et al. 2007). In our study we did not investigate pollen distributions because of the small lateral extent of the present day mangroves. The present-day mangrove vegetation is zoned with respect to tidal levels, but pollen would likely provide little additional information beyond that given by using the upper and lower limits of mangrove vegetation as our primary sea-level indicator.

Our dating strategy for mangrove sediment was initially based on AMS ^{14}C dating of bulk sediments. However previous studies of fossil mangrove sediments show that where mangrove environments are established for any length of time younger mangrove roots will penetrate the older underlying sediments. The introduction of young carbon down-profile means that bulk AMS ^{14}C ages on mangrove peat are often young compared with the true age of deposition (e.g. Smith and Coleman 1967; Schofield 1977; Woodroffe 1981; Woodroffe 1988b; Woodroffe 1990).

To assess whether the incorporation of young carbon down-profile was a function of different material being dated, we obtained an additional pair of dates from 1 m depth in Anse Boileau core 4 on fine root hairs and larger pieces of wood that we assumed to be root material. The fine root hairs dated to c. 900 cal yr BP and woody material to c. 1450 cal yr BP (the bulk age from the same depth was modern, Table 1). Although the woody material has the oldest age, because we have no independent chronohorizons in our sediment cores we have no way of knowing if this is the true age of the deposit. The results of this comparison suggest that dating large wood fragments may yield older and more reliable ages compared to bulk sediments or fine root hairs in this location (although we note that this is only based on one paired sample). This observation does not accord with the notion of large younger mangrove roots penetrating older sediment. From this test we conclude that it is the fine root hairs that are the probable source of young carbon and that ^{14}C-derived ages of bulk sediments provide minimum ages for sea-level reconstruction. There are other approaches that researchers have taken to dating sediments with multiple carbon sources, and it may be that by using a particular size fraction of organic material (as described above) or pollen concentrates in the future, we could resolve the other reversals seen in the bulk sediment ages and extend the existing record further back in time (e.g. Vandergoes and Prior 2003; Newnham et al. 2007; Li et al. 2014; Woodroffe et al. 2015).

To provide a maximum age for the formation of the plateau fossil beach at Barbarons we conducted ^{14}C and Uranium-Thorium dating on fragments of coral extracted from cores from within the plateau beach deposits (Figure 2B and Tables 1 and 2). All AMS ^{14}C dating was undertaken at the NERC Radiocarbon Facility and SUERC AMS Laboratory at East Kilbride, Scotland. We calibrated the ^{14}C ages using Oxcal version 4.2 (Bronk Ramsey 2009) using SHCal13 (Hogg et al. 2013) for terrestrial and mangrove samples, and MARINE13 for coral samples (Reimer et al. 2013) using a ΔR of 140 ± 25 (Southon et al. 2002). All calibrated ^{14}C ages are cited with a 2 sigma age range (Table 1). Uranium-Thorium dating on coral fragments from the plateau at Barbarons was performed on a Nu-Instruments multicollector inductively coupled plasma mass spectrometer at the University of Oxford. Approximately 0.3g or coral was cleaned by ultrasonicating in 18 MΩcm water. The samples were spiked with a mixed ^{229}Th-^{236}U tracer solution; dissolved and then organic material removed with aqua-regia; before U and Th were isolated from the sample matrix by anion chromatography (Edwards et al. 1987). Uranium isotopes were measured by standard bracketing against the CRM-145 standard while Th isotopes were measured against an in-house ^{229}Th-^{230}Th-^{232}Th standard (Mason and Henderson 2010). Data and ages are presented in Table 2. The elevated ^{232}Th concentrations indicate the presence of detrital material within the coral skeleton which will incorporate initial ^{230}Th and ^{234}U, which would otherwise bias ages towards older values. Ages have been calculated with a correction for this initial component assuming a crustal composition (Table 2).

3.2 Glacial-Isoststatic Adjustment model

The GIA sea-level model applied here solves the sea-level equation that incorporates changes in shoreline position (Mitrovica and Milne 2003; Kendall et al. 2005) and includes the influence of GIA-induced changes in Earth rotation on RSL (Milne and Mitrovica 1998; Mitrovica et al. 2005). Model results were computed using two different reconstructions of global ice evolution from the last interglacial through to the present day (ICE-5G and EUST3). The Earth model used is a spherically-symmetric, self-gravitating, Maxwell visco-elastic body in which the viscous structure is defined by three parameters: thickness of an outer layer (the model lithosphere) in which the viscosity is assigned very high values such that it acts elastically over GIA timescales; uniform viscosity in the upper (base of lithosphere to 660 km depth) and lower (660 km to core-mantle boundary) mantle regions. These three parameters were varied in the modelling described below. The elastic and density structure of the Earth model were taken from seismic constraints (Dziewonski and Anderson 1981) and depth parameterised with greater resolution (~100 layers in the mantle region) compared to the 3-layer viscous structure defined above. The elastic and density values were not varied in the results shown below.

4.Results

We investigated the coastal geomorphology and mangrove environments at Barbarons, the mangroves at Anse Boileau and coastal geomorphology at Anse a la Mouche. The results bring together a range of sea-level indicators at these locations from the morphology and age of plateau fossil beaches, modern reef deposits and fossil mangrove sediments which record changes in the height of RSL through the late Holocene. The main RSL indicator used is mangrove sediments.

4.1 Barbarons

4.1.1 Plateau and reef data from Barbarons

Barbarons, on the west coast of Mahé, is a c. 850 m wide bay fronted by fringing reef, with a modern beach backed by plateau and mangroves (Figure 1C). We collected and dated using U-Th and AMS radiocarbon detrital coral fragments (all 2-5 cm in length) from cores taken towards the rear of the plateau in transects 1 and 3. These yield ages that vary between c. 4.5-1.6 ka cal BP (Tables 1, 2 and Figures 1C, 2A and 2B). Two samples from the same depth in a single borehole vary by up to c. 1.8 ka (Table 1). There is general agreement between the ^{14}C and U-Th ages (Figure 4B). The overall age variability is expected given that the dated material is reworked and our objective here was to establish the youngest age of the samples to establish a maximum age for the plateau formation. The youngest age is c. 1650 cal yr BP, indicating that the plateau is a relatively recent element of the coastal landscape that accreted in the last 1.5 – 2 ka.

The surface of the plateau is relatively flat across the two shore-normal survey transects at Barbarons (Figure 2A), and this is also repeated in a different bay on the west coast of Mahé (Anse a la Mouche, Figure 3). The plateau surface is c. 1.6 m above HAT at the north end of Barbarons (Transect 3) and 0.8 m above HAT at the south end (Transect 4). This mirrors the decrease in elevation of the modern beach crest between the north and south ends of the bay, and reflects the attenuation of wave energy within the bay. The plateau surface is consistently 0.2-0.6 m below the immediately adjacent present day storm beach crest (Figure 2A). The uniform nature of its topography and the fact that in no location is this feature higher than the present day storm beach crest suggests that the plateau formed under relatively stable RSL, although we cannot rule out some post-depositional modification by human activities.

To establish an age for the fringing reef flat at Barbarons, we collected three samples of cemented coral material for U-Th dating using a hand-operated rotary drill corer from the reef surface immediately in front of the modern beach, c. 50 m landward of the living reef edge (Figures 1C and 2A). Two of these samples have low Uranium concentrations (less than 1ppm), which suggests they may have lost Uranium and we treat these ages with caution. The third sample yielded a modern age. This is not wholly unexpected as the fringing reefs around Seychelles are dominated by storm deposits that are mobilised at the reef edge and

travel across the reef flat, and may then become re-cemented over time (Braithwaite et al. 2000; Kennedy and Woodroffe 2002). Surface reef-flat ages in this location therefore represent deposition from modern storms and not the timing of lateral reef flat accretion during the late Holocene.

4.1.2 Mangrove sea-level data from Barbarons

Fossil mangrove sediments are preserved in the channel of the River Dauban, which cuts through the plateau at the north end of Barbarons and meets the sea at Grand Anse (Figure 1C). Coring transects completed across the River Dauban mangroves reveal a relatively consistent stratigraphy, comprising a lower unit of sand that becomes increasingly organic up core, overlain by a dense peat with frequent fine rootlets and wood fragments, which locally grades upwards into a sand-rich peat and is overlain abruptly in the top 30 cm or so by coarse organic sand that extends to the present surface. We interpret this stratigraphy as recording initial colonisation of river-mouth sand deposits by mangrove, which infilled available accommodation space. The origin of the coarse sand on the top of the mangrove deposits here and elsewhere on Mahé is uncertain; it could represent a local change in coastal morphology, a recent increase in terrigenous sediment delivery to the mangroves, the effects of recent RSL change, or an abrupt event such as the impact of a far-field tsunami.

We ^{14}C dated the fossil mangrove in three sediment cores (mangrove cores 1, 2 and 3, Figures 1C, 2A, B, Table 1). The oldest age is from core 2 (2757-2493 cal yr BP at 0.75 m, Table 1) but this is out of sequence with ages from the lower down the same core. This may be because mangrove roots have introduced young carbon towards the base of this core or because this age includes old carbon from allochthonous organic material brought to the sample site from upstream sources in the catchment. We cannot resolve which of these hypotheses is most probable and assume that the bulk age on the base of this core (1722-1544 cal yr BP) is reliable because it broadly corresponds to the basal age of mangrove core 4 at Anse Boileau, which is at a similar elevation (Table 1).

Using the modern day limits of mangrove vegetation we reconstruct RSL at Barbarons to a maximum of c. 2 m below present between 2-1 ka cal BP, and rising to present in the last 1 ka (Figures 4A and B, Table 1). There is no evidence here for RSL above present in the last 2 ka.

4.2 *Anse Boileau*

4.2.1 Mangrove sea-level data from Anse Boileau

Anse Boileau is 4 km southeast of Barbarons and mangrove sediments here surround the outflow of the River Cayman (Figure 3A). The deposits have a very similar stratigraphy to those at Barbarons. The lowest

unit is coarse granitic sand which grades upwards into sandy and root-rich peat that is overlain abruptly in the top 30 cm by coarse sand (Figure 3A). We interpret this stratigraphy similarly to that at Barbarons as evidence for the establishment of mangroves over a river-mouth sand with a more recent switch to sand deposition near the surface. Four AMS ^{14}C ages from mangrove peat in core 4 all overlap, suggesting either very rapid sediment accumulation or mixing of carbon sources (Table 1). All the ^{14}C ages on mangrove deposits in this core are younger than 2 ka cal BP, although the problem of younger mangrove roots penetrating into older deposits means that the mangroves here may have formed prior to this date. However the relatively high energy nature of this coastline means that mangrove formation likely required the establishment of the plateau sand barrier, and as noted above, our dating evidence suggests that this was likely in place by 2 ka cal BP. This lends weight to the suggestion that the mangrove peats also formed after this date. Using the modern day limits of mangrove vegetation measured here and at Barbarons we reconstruct RSL to a maximum of c. 2 m below present between 2-1 ka cal BP. There is also no evidence for RSL above present in the last 2 ka.

4.3 Anse a la Mouche

4.3.1 Plateau and reef evidence from Anse a la Mouche

Anse a la Mouche is approximately 4 km southeast of Anse Boileau (Figure 1B). Any former mangrove habitats in this bay have now been reclaimed and we therefore only investigated the morphology of the plateau and reef flat. The plateau surface here is very regular and, as at Barbarons, sits approximately 10-15 cm below the height of the modern storm beach crest (Figures 2A and 3B). The uniform nature of the topography suggests that the plateau at both locations formed under relatively stable RSL. No other data was collected from this site.

4.4 Potential for post-depositional compaction of mangrove sediments through time

Compaction of fossil organic deposits through time can be an important issue when reconstructing RSL using intertidal sediments. Compaction-induced lowering of sea-level index points from the elevations at which they were deposited distorts age-altitude relationships (Horton and Shennan 2009; Brain et al. 2012). It has been suggested that measurements of bulk density can be used to determine whether compaction has occurred on the assumption that a downcore increase in bulk density is indicative of compaction and, hence, post depositional lowering (Gehrels et al. 2006; Kemp et al. 2009). However, this method is not suitable in stratigraphies such as ours where variations in lithology make identifying downcore trends in bulk density difficult (Brain et al., 2012). Ideally we need a detailed site- and lithology-specific understanding of mangrove compaction processes but this is beyond the scope of this study (Brain

et al., 2015). Bird et al. (2004) proposed a method of estimating compaction in mangroves by comparing the dry bulk density of modern mangrove sediment deposits with fossil sediments, and by scaling volume, and hence layer thickness, accordingly. They suggest that mangrove muds (up to 50 % LOI on the < 63 µm size fraction) may compact by up to 30 % in a 2 m stratigraphic column. This method is likely to overestimate the magnitude of thickness change because compaction is a gradual, cumulative process that is a function of the depth of underlying material and the stress applied by the overburden (Tornqvist et al. 2008; Horton and Shennan 2009). Full 'decompaction' throughout a stratigraphic column does not consider intermediate states of compaction between surface and *in situ* conditions.

We acknowledge that there is likely to have been some compaction in the mangrove sediments at Barbarons and Anse Boileau. In the absence of a more detailed geotechnical correction method, we adopt the approach of Bird et al. (2004), who suggested that the maximum potential compaction in their analysed sequence most similar to ours is 30 % over 2 m (c. 60 cm). It is very likely that compaction of the mangrove sediments on Mahé has been less than this because our sediment cores are shorter (up to 1.65 m to the base of the peat) and are much younger (last 2 ka compared to last 7 ka for Bird et al.'s sediments). Relative sea-level reconstructions from the basal section of the cores from Barbarons and Anse Boileau do sit slightly low compared to predicted RSL from two GIA models (Figure 4B), however raising these reconstructions by c. 0.6 m (assuming the worst-case compaction scenario suggested by Bird et al. 2004) we would still not be able to differentiate between the two end-member GIA model predictions in this location during the last 2 ka (Figure 4B).

4.5 Late Holocene RSL and coastal evolution on Mahé

We combine data from Barbarons, Anse Boileau and Anse a la Mouche, with Braithwaite et al.'s (2000) coral data from Anse aux Pins to reconstruct late Holocene RSL and coastal evolution on Mahé. As noted above, most of the coral data is of poor quality for reconstructing RSL because the dated coral is not *in situ* and is likely to have been transported during storms onto the reef flat surface (Figure 4A and B). The most reliable index points come from *in situ Acropora danai* framework reef, which is today found in the high energy reef front and upper forereef zone of SW Indian Ocean fringing reefs, and lives in a 6 m window below LAT (Camoin et al. 1997; Montaggioni and Faure 1997; Cabioch et al. 1999). However there are only four index points in the past 10 ka which come from this species of framework coral (Figure 4A).

The coral data record rapid RSL rise during the early Holocene from between 15-7 m below present at c. 9.5 ka cal BP, with the youngest age (from coral debris 1.8 m below the modern reef flat) of c. 3.7 ka cal BP providing an estimate of when RSL reached present (Figure 4A). Camoin et al. (2004) propose that RSL stabilisation across the SW Indian Ocean occurred around 1000 years after this date, between 3-2.5 ka cal

BP. Braithwaite et al. (2000) suggest their age for reef stabilisation on Mahé represents the broad timing of when RSL reached present, but as their youngest date is from 1.8 m below the modern reef flat surface it provides only a maximum age for this event.

Our dates from the plateau at Barbarons show that sand began to accrete after 2 ka cal BP. Plateau formation would only have occurred once the adjacent fringing reef flat was close enough to sea level to provide both a local source of sand and reef material, and a platform for the sand to accrete onto. We hypothesise that the fringing reef took centuries to millennia to "catch-up" to sea level in the late Holocene, explaining the delay between the youngest coral age of Braithwaite et al. (2000) (c. 3.7 ka cal BP), Camoin et al.'s (2004) estimate of regional RSL stabilisation (3-2.5 ka cal BP) and our chronology for the deposition of the sand plateau on Mahé (after 2 ka cal BP). We suggest that mangrove formation was only possible once the plateau had begun to accumulate, as it provided the necessary quiet-water protection and accommodation space within which intertidal mangroves could become established.

The overlapping nature of the ^{14}C ages from the mangrove horizons within cores from both Barbarons and Anse Boileau indicate that once coastal mangrove sediments had started to accumulate after 2 ka cal BP, there was a rapid infilling of available accommodation space leading to c. 1.4 m (or more, depending on sediment compaction estimates) of mangrove peat accumulating in less than 1000 years (Figure 2B and 3A). This rapid infilling of accommodation space is reminiscent of the 'big swamp phase' of rapid mangrove expansion during RSL slow-down and stabilisation seen elsewhere in the Indo west-Pacific during the mid-Holocene (Woodroffe et al. 1985; Woodroffe 1988a). However in Seychelles it appears that because of the high energy nature of the coastline, the development of the plateau was necessary to provide the right conditions for mangroves to grow on Mahé, rather than mangrove expansion being driven predominantly by RSL slow-down.

Our radiocarbon ages on mangrove sediments provide new minimum ages on late Holocene RSL changes. RSL had risen to within c. 2 m of present by 2-1 ka cal BP. Our interpretation of RSL change is by necessity generalised because of problems with dating mangrove sediments discussed above and the lack of microfossil data. These mangrove dates are minimum ages so it is possible that RSL reached c. 2 m below present before 2 ka cal BP. Because of the elevation and age errors associated with the mangrove RSL data and the lack of dated material from before 2.7 ka cal BP we cannot say conclusively when RSL first reached close to present. However the ages for plateau formation from detrital coral give us confidence that RSL was certainly within c. 2 m of present during the last 2 ka.

There is no evidence for a late Holocene highstand at any of the locations studied on Mahé, although the widespread occurrence of coarse organic sand in the top 30 cm or so of mangrove sediments at Barbarons

and Anse Boileau suggests that there has been a recent change in coastal sedimentation. One explanation for this change is that it records the effects of the 2004 Indian Ocean tsunami which caused widespread damage on Mahé, particularly to east-facing shores but also caused coastal flooding and structural damage on the west coast of Mahé. Jackson et al. (2005) suggested that tsunami run up associated with this event was c. 3.25 m above HAT at Grand Anse, just north of Barbarons, and c. 1.45 m above HAT at Anse Boileau. The mangroves in these locations were inundated by the tsunami waves which may have caused the erosion of the active mangrove peat surface and the deposition of a sand layer. An alternative explanation is that the coarse sands record recent terrigenous sediment influx as a result of intensive development of the interior of Mahé. The coarse, granitic nature of the sand, coupled with a lack of detrital carbonate remains within the sand, would favour this over the tsunami hypothesis.

4.6 Optimising the earth model and estimating eustatic sea level

The next step in our analysis is to remove the GIA signal from the RSL data in order to estimate late Holocene eustasy. We start by comparing our data to RSL predictions from two different GIA models (ICE-5G and EUST3) to define an optimal earth viscosity for each model in this location. For ICE-5G, all viscosity parameter combinations (lithospheric thicknesses of 71, 96 and 120 km, upper mantle viscosities of 0.05, 0.08, 0.1, 0.2, 0.3, 0.5, 0.8, 1, 2, 3 and 5 x 10^{21} Pas and lower mantle viscosities of 1, 2, 3, 5, 8, 10, 20, 30 and 50 x 10^{21} Pas) have chi-squared values within the 95 % confidence limit (Figure 5A). In comparison, for EUST3, the full range of lower mantle viscosities are accepted at this level of confidence, although only relatively high/low values of upper mantle viscosity produce acceptable fits (Figure 5B). The results for EUST3 using different lithospheric thicknesses were similar but the lowest chi-squared values were obtained with thinner lithosphere models in general. The optimal earth model for both ICE-5G and EUST3 has a lithospheric thickness of 71 km, an upper mantle viscosity of 0.5 x 10^{20} Pas and a lower mantle viscosity of 3 x 10^{21} Pas. The difference in the Seychelles GIA correction using ICE-5G or EUST3 is small since 4 ka BP (maximum difference ~0.5 m) whichever earth viscosity profile is chosen, as one would expect given the results of Milne and Mitrovica (2008). However the magnitude of the difference increases further back in time, with a difference of ~2.7 m between the model corrections at 9.7 ka BP.

We removed the GIA signal from the RSL data using the two best-fitting earth models defined above. Figure 4 shows data with the non-eustatic signal from the best-fitting GIA models removed (ICE-5G in Fig. 4C and EUST3 in 4D). The GIA corrections using either model are relatively small, although those for EUST3 are larger than for ICE-5G in the last 4 ka because of the GIA effects associated with its larger late Holocene eustatic contribution. The largest GIA correction made to the oldest mangrove data is 0.52 m (EUST3) and 0.31 m (ICE-5G) (mangrove core 2, Table 3). The vertical uncertainties in the model-corrected reconstructions combine both data and model uncertainties in quadrature. The model uncertainty is simply

the spread of values obtained using all predictions that satisfied the 95% confidence cut-off based on an F-test. Comparison of the model-corrected data in Figures 4 C and D indicates that the results obtained for the two ice models are very similar. In all cases the data uncertainties associated with defining the indicative meaning of the mangrove sea-level indicators dominate the total error (Table 3).

The model-corrected data indicate that eustatic sea level rose through the early-mid Holocene, reaching within c. -2 m of present before c. 2 ka cal BP. The exact timing of sea level first reaching within -2 m of present is poorly constrained because of a data gap between the youngest coral age (c. 3.7 ka cal BP (Braithwaite et al. (2000)) and the oldest mangrove ages from this study (c. 2.7-2 ka cal BP). Errors on the mangrove reconstructions make it impossible to identify the nature of sea-level variability within the -2 to 0 m window since 2 ka cal BP, although the model-corrected data suggest that eustatic sea level remained within this vertical range and did not rise more than a few decimetres above present during that time.

5 Discussion

5.1 Comparing sea-level data and model predictions of RSL change during the Holocene

During the early Holocene, the coral index points from Braithwaite et al. (2000) and GIA model predictions do not agree. The GIA models predict RSL was around -20 m at c. 9 ka cal BP and rising very quickly during this period, whilst the coral data suggest RSL was between -11 and -6 m and rising more gradually (Figure 4A). RSL changes in this region are dominated by the eustatic contribution, and the GIA correction is relatively small (between 0.4-2.3 m around 9.7 ka cal BP depending on which ice model is chosen, Table 3). This suggests that either the coral data from this period (framework coral and coral debris) are not *in situ* or that eustatic rise occurred earlier than is predicted by the GIA models. We hypothesise that the storm-dominated coral reef setting on Mahé means that the coral index points from this period most likely consist of reworked material that was transported onto a more recent and higher reef flat surface and that the coral-based RSL data from this period are not reliable.

During the mid-Holocene the coral index points from Braithwaite et al. (2000) and the GIA model predictions broadly agree on the timing and rate of RSL rise (Figure 4A), although we note that the age and elevation uncertainties on the coral reconstructions do not provide a good test of the model. The youngest coral data is c. 3.7 cal ka BP and suggests that RSL was close to present by this time, within error (± 3-4 m). The coral data cannot help us to discriminate between RSL predictions from ICE-5G, which predicts RSL to be ~-1 m at 4 ka cal BP, and those from EUST3 which predicts RSL at ~-2.5 m at this time. Our new mangrove data fill an important data gap during the late Holocene in the last 2 ka and, together with the

morphological and dating evidence from the plateau, suggest that RSL was between -2 m and 0 m during this period and did not rise above present.

5.2 Processes in the GIA correction

Camoin et al. (2004) hypothesise that continued late Holocene RSL rise in Seychelles (and in other locations in the southwest Indian Ocean) is because this region experienced late Holocene hydro-isostatic sea-floor subsidence after the end of major ice sheet melting in the mid-Holocene. They compare the situation here to that in the Caribbean, where continued late Holocene RSL rise is attributed largely to the collapse of the former Laurentide ice sheet forebulge (Milne et al. 2005; Milne and Peros 2013). The results in Figure 6 indicate that the situation in the southwest Indian Ocean is similar to that of the Caribbean but the forebulge collapse due to ice unloading (Fennoscandian ice) is less prominent given the larger distance from the ice sheet in this case. Note that, for each ice model considered, the influence of syphoning is of similar magnitude but opposite sign to the combined RSL signal due to ice and ocean loading effects (on both the sea surface and sea floor). During the late Holocene the ice and ocean loading signals, which are primarily due to sea floor subsidence, slightly dominate that from syphoning and so the total predicted RSL curve sits slightly below the model eustatic curve. We note that the ice-load component of the signal is about 30% larger than the ocean-load component during the late Holocene.

5.3 Late Holocene eustasy

Because the non-eustatic GIA component of RSL is modelled to be small in Seychelles compared to most other coastal locations around the world (Milne and Mitrovica, 2008), new late Holocene sea-level data should, in principle, help us to accept or reject the eustatic functions in different GIA models. In Figures 4C and D we show that the estimated eustatic sea level was close to or at present by c. 2 ka cal BP regardless of which ice model was used in calculating the GIA corrections. The GIA corrections calculated using ICE-5G and EUST3 are small in the last thousand years (0.1-0.2 m ± 0.04-0.2 m), but are closer in magnitude to the observed sea-level changes by 2 ka cal BP (Table 3). Therefore despite this location being chosen to minimise any late Holocene GIA correction, the correction and its uncertainty are still important, even though the latter is smaller in magnitude than the RSL reconstruction uncertainties.

Overall uncertainty in estimating eustasy is a calculated based on the uncertainty in both the RSL reconstruction and GIA model correction (these two sources of uncertainty are combined in quadrature). This net uncertainty, which ranges from ± 0.6 to 0.89 m for the mangrove data, makes it relatively difficult to choose between the two eustatic models presented in Figure 4C and 4D, because the

predictions for each model differ by only a decimetre or so during the period spanned by the data (2 ka BP to present). However, the eustatic component of the EUST3 model better captures the cluster of data points between 2 and 1.5 ka BP and so is marginally preferred by the observations.

We further hypothesise that eustasy likely first reached within -2 m of present in the 1.7 ka interval between the end of the coral and start of our mangrove record, c. 3.7-2 ka cal BP. We also conclude that it is unlikely that there were metre-scale RSL oscillations during the period between 2 ka cal BP and present. This result is closer to the eustatic function in EUST3 which includes 1.5 m of melt since 4 ka cal BP than that of ICE-5G which predicts close to zero eustatic sea level change after 4 ka cal BP. However, we conclude that the timing of when eustatic sea level first rose close to present is between the predictions of the two end-member models presented here (4 ka cal BP for ICE-5G and 1 ka cal BP for EUST3).

Evidence from archaeological remains and other palaeo sea-level indicators from elsewhere in the world also suggest negligible eustatic contribution in the last 2 ka. Archaeological evidence from the Mediterranean region, based in part on the interpretation of Roman fish tanks and also coastal wells in Israel, indicate little net RSL change since the Roman period (Lambeck et al. 2004; Sivan et al. 2004; Lambeck and Purcell 2005; Sivan et al. 2010; Anzidei et al. 2011; Toker et al. 2012), as does a recently published 2 ka-long record of RSL change from northwest Scotland based on salt marsh data (Barlow et al. 2014). Lambeck and Purcell (2005) also suggest, from evidence in the Mediterranean, that the eustatic contribution ended at around 3 ka cal BP and Lambeck et al. (2014) indicate that eustasy was within 0.5 m of present by 3 ka cal BP, both of which agree with our observations from Seychelles. Sea-level data from microatolls on Christmas Island in the Pacific record no oscillations greater than 0.25 m since 5 ka cal BP although this location does not closely track eustasy and requires a metre-scale GIA correction in the late Holocene (Woodroffe et al. 2012).

These observations indicate that the polar ice sheets, notably Greenland and Antarctica, must have been relatively “stable” during at least the last 2 ka in terms of their combined contribution to eustatic sea level. As discussed above, Greenland likely gained a modest amount of mass during the neoglacial period, reaching close to its Holocene maximum extent at the end of the Little Ice Age and with a modelled draw-down of less than c. 0.2 m during the last few thousand years (Simpson et al. 2009; Lecavalier et al. 2014). The late Holocene ice mass history of Antarctica is, compared to Greenland, poorly constrained with considerable uncertainty. Palaeoclimate data from a range of proxies suggests that there was a period of late Holocene warmth from between c. 4-2 ka cal BP (e.g. Bentley et al. 2009; Sterken et al. 2012; Hodgson and Bentley 2013), which coincided with a peak in late Holocene austral annual insolation (Marcott et al. 2013). This warmth appears to have ended around 2 ka cal BP. There is also some evidence that at least parts of Antarctica have melted throughout the Holocene, with melt continuing in Marie Byrd Land until at

least c. 2400 cal yr BP (Stone et al. 2003), which fits with the period of late Holocene warmth reconstructed from palaeoclimate proxies. , Considering evidence from Greenland and Antarctica there is currently no suggestion from geological archives that either ice sheets lost significant mass in the last 2 ka (in the range of 1-2 m eustatic contribution) or fluctuated in mass by this magnitude. From our far-field sea-level analysis it would seem that eustasy has been relatively insensitive to climate fluctuations during the pre-industrial part of the last 2 ka.

To improve RSL and eustatic sea-level reconstructions in Seychelles requires new RSL data from the mangroves on Mahé (with improved dating control) and alternative proxies from this area, such as coral microatolls that have small vertical uncertainties (e.g. Woodroffe et al., 2012). It would be especially helpful to fill the current data gap between the youngest cored coral and the oldest mangrove index points to pinpoint better when eustatic sea level first came within -1.5 m of present. Even with additional data it will, however, be challenging to produce RSL reconstructions with sufficient precision to fully discriminate between the two ice models considered in this paper.

In a wider context, more late Holocene sea-level data from the western Indian Ocean region using high resolution indicators would also help to characterise the impact of water mass distribution caused by changes in atmospheric and ocean circulation due to the El Nino Southern Oscillation, Indian Ocean Dipole and Asian-Australian monsoon on decadal-centennial sea-level trends (Church et al. 2006). This would allow us to further refine the eustatic function in these RSL records.

6 Conclusions

This study was designed to provide precise estimates of globally integrated ice sheet melt during the late Holocene from a location where the necessary GIA correction is small and relatively insensitive to predictions using different Earth viscosity profiles (Milne and Mitrovica, 2008). Using a combination of mangrove sediments and coastal geomorphology on Mahé, Seychelles, we have extended the existing coral-based RSL record into the late Holocene and provided new constraints on eustasy during this period. These constraints include uncertainty associated with both model parameters (ice and Earth model viscosity structure) and the sea-level reconstructions. In this case, the latter dominate the eustasy estimates.

Our main conclusions are:

1. Seychelles is well situated for investigating globally integrated ice-sheet melt because of its location in the far field in a region that is modelled to closely track eustasy during the late Holocene, and because

of its relative tectonic stability. There are coastal environments around the main granitic islands, particularly on Mahé, which preserve evidence of RSL changes through much of the Holocene.

2. Existing coral data suggest that RSL rose continually through the early-mid Holocene, and reached close to present by c. 3.7 ka cal BP, although the error terms on these reconstructions are large (± 3-4 m).
3. Plateau deposits of carbonate-rich sand at Barbarons on the west coast of Mahé formed in the last 2 ka and the horizontal surface topography of these deposits suggests RSL stability during this time.
4. Extant and reclaimed mangrove sediments are preserved behind the plateau and in river mouths around Mahé. These deposits formed since c. 2-1.5 ka BP and indicate that RSL was between -2 m and present during this period. Down-profile contamination by younger carbon of unknown provenance makes development of ^{14}C chronologies from these deposits difficult.
5. The overall pattern of GIA-corrected (eustatic) sea level on Mahé is one of sea level rise through the early and mid-Holocene, reaching within c. -2 m of present in the late Holocene. The exact date when sea level first reached within -2 m of present is sometime between 3.7 and 2 ka cal BP. Eustatic sea level remained within -2 m of present after this time and has not risen more than a few decimetres above present during the last 2 ka. This result adds support to the eustatic function in EUST3 which includes 1.5 m of melt since 4 ka cal BP, rather than that of ICE-5G which assumes that eustatic sea level reached present by 4 ka cal BP.
6. Using all lines of RSL evidence currently available from Mahé we suggest that the eustatic contribution during the last 2 ka has been negligible. That this conclusion is drawn from a tectonically stable, far-field region that is relatively insensitive to earth and ice model uncertainties adds weight to geological observations from the polar ice sheets that suggest that they lost limited mass to the oceans during the last 2 ka. This implies that global eustasy has been relatively insensitive to climate fluctuations during the pre-industrial part of the last 2 ka

Acknowledgements

This paper is a contribution to PALSEA2, IGCP 588 and the INQUA Commission on Coastal and Marine Processes. The work was supported by the NERC Radiocarbon Facility NRCF010001 (allocation number 1424.1009). We thank Colin Murray-Wallace and two anonymous reviewers whose comments significantly improved the manuscript.

Figure captions

Figure 1. A) map of the southwest Indian Ocean showing the location of the main granitic islands of the Seychelles and other locations mentioned in the text, B) map of the island of Mahé showing the location of the sites investigated in this study and the previous fringing coral study of Braithwaite et al. (2000) – Anse aux Pins, C) detailed map of the Barbarons area showing the coastal geomorphology and the location of transect lines, cores and samples taken for ^{14}C and U/Th dating.

Figure 2. A) two transect lines across the plateau at Barbarons, showing the elevation of the reef flat, beach and plateau with wetland behind, and local tidal levels. Also shown are the U/Th ages from detrital coral samples taken from the base of cores in the plateau and ^{14}C ages from mangrove sediments located behind the plateau at Barbarons, B) detailed stratigraphy from transects 1 and 2 taken through mangrove sediments at the northern end of Barbarons. Transect 1 shows ^{14}C ages on detrital coral from within the plateau as well as ages on mangrove deposits in core 1. Transect 2 has one dated core (mangrove core 2).

Figure 3. Mangrove sediments investigated and dates from a core at Anse Boileau and a transect taken through the plateau at Anse a la Mouche (see Figure 1 for their locations).

Figure 4. A) Holocene RSL data from cored coral (framework and coral debris) and mangrove sediments on Mahé. Also shown are RSL predictions from two global ice model reconstructions; ICE-5G and EUST3, using earth models that provided a best-fit to the mangrove-based sea-level data. In both cases the optimal earth model has a lithospheric thickness of 71 km, an upper mantle viscosity of 0.5×10^{20} Pas and a lower mantle viscosity of 3×10^{21} Pas. The index point drawn using dashed lines is from an out of sequence age in Mangrove core 2 which may record RSL close to present as early as c. 2.7 ka cal BP. B) Mid-late Holocene RSL data from Mahé and geophysical model RSL predictions (as in part A) and also the ages of detrital coral fragments found in plateau cores at Barbarons (see Figures 1C, 2A and 2B for the location of the analysed samples). C) Mid-late Holocene sea level data from Mahe corrected for GIA using the suite of optimal ICE-5G model predictions (details in main text). Also shown is the ICE-5G global eustatic function through time for comparison. D) GIA-corrected sea-level data as in C but using the optimal suite of EUST3 model results (details in main textabove). Also shown is the EUST3 global eustatic function through time for comparison.

Figure 5. Chi-squared plots for (A) ICE-5G and (B) EUST3 demonstrating the goodness of fit of RSL predictions using a 71 km thick lithosphere with a range of upper and lower mantle viscosities to the mangrove-based RSL data. For the EUST3 results (B), chi-squared values less than 1.56 define solutions that are within the 95 % confidence limit using an F-test. All viscosity models considered using a 71 km thick lithosphere for the ICE-5G model (A) are within the 95 % confidence limit.

Figure 6. The contribution of different GIA processes to RSL predicted by (A) ICE-5G and (B) EUST3 during the mid to late Holocene on Mahé. The different curves are as follows: 'RSL' is the total RSL for this location (which includes all GIA processes and includes eustasy); 'Eustasy' is the meltwater contribution to global mean sea level; 'Syphoning' is the contribution from syphoning (a global mean signal; see text for details); 'Ice' is the contribution of ice loading only to RSL (including sea surface and ocean floor components); 'Ocean' is the contribution of ocean loading only to RSL (including sea surface and ocean floor components). Note that the RSL contribution from GIA-induced changes in earth rotation are included in the total (RSL) but are not shown on the figures because the values are small.

Table 1. ^{14}C ages on mangrove sediments and coral fragments from Barbarons. All altitudes were surveyed using a level and staff with closed levelling transects that are tied to a common reference point that we related to MTL using hourly tide gauge readings for Pt. la Rue, Mahé. All AMS ^{14}C dating was undertaken at the NERC Radiocarbon Facility and SUERC AMS Laboratory at East Kilbride, Scotland. We calibrated all ^{14}C ages using Oxcal version 4.2 (Bronk Ramsey 2009) using SHCal13 (Hogg et al. 2013) for terrestrial, mangrove samples and MARINE13 for coral samples (Reimer et al. 2013) using a ΔR of 140 ± 25 (Southon et al. 2002). All calibrated ^{14}C ages are cited with a 2 sigma age range. * Repeat measurement using additional pre-treated sediment which was conducted as an additional check on results. The duplicate results agree within 2 sigma confidence limits.

Table 2. U and Th concentrations, isotopic composition (as activity ratios) and ages from coral fragments and lithified reef flat samples from Barbarons (see Figure 1 for their locations). Ages are calculated with Isoplot v. 4.15 (Ludwig 1991) using a correction for detrital "initial" ^{230}Th and ^{234}U based on an approximate crustal composition. Ages are presented as calendar years prior to AD1950. $(^{234}U/^{238}U)_0$ is the $(^{234}U/^{238}U)$ of the coral corrected for decay since deposition and detrital U.

Table 3. RSL reconstructions from coral and mangroves on Mahé and glacial-isostatic adjustment corrections applied to the data to produce eustatic estimates.

References

(Admiralty Tide Tables 2009) NP203 Admiralty Tide Tables (ATT) Volume 3, Indian Ocean and South China Sea (including Tidal Stream Tables)

Anzidei M, Antonioli E, Benini A, Lambeck K, Sivan D, Serpelloni E, Stocchi R (2011) Sea level change and vertical land movements since the last two millennia along the coasts of southwestern Turkey and Israel. Quatern Int 232: 13-20 doi DOI 10.1016/j.quaint.2010.05.005

Barclay DJ, Wiles GC, Calkin PE (2009) Holocene glacier fluctuations in Alaska. Quaternary Sci Rev 28: 2034-2048 doi DOI 10.1016/j.quascirev.2009.01.016

Bard E, Hamelin B, Arnold M, Montaggioni L, Cabioch G, Faure G, Rougerie F (1996) Deglacial sea-level record from Tahiti corals and the timing of global meltwater discharge. Nature 382: 241-244

Barlow NLM, Long AJ, Saher MH, Gehrels WR, Garnett MH, Scaife RG (2014) Salt-marsh reconstructions of relative sea-level change in the North Atlantic during the last 2000 years. Quaternary Sci Rev 99: 1-16

Bentley MJ, Hodgson DA, Smith JA, Cofaigh CO, Domack EW, Larter RD, Roberts SJ, Brachfeld S, Leventer A, Hjort C, Hillenbrand CD, Evans J (2009) Mechanisms of Holocene palaeoenvironmental change in the Antarctic Peninsula region. Holocene 19: 51-69 doi Doi 10.1177/0959683608096603

Bird MI, Fifield LK, Chua S, Goh B (2004) Calculating sediment compaction for radiocarbon dating of intertidal sediments. Radiocarbon 46: 421-435

Bradley SL, Milne GA, Shennan I, Edwards R (2011) An improved Glacial Isostatic Adjustment model for the British Isles. Journal of Quaternary Science 26: 541-552 doi Doi 10.1002/Jqs.1481

Brain MJ, Long AJ, Woodroffe SA, Petley DN, Milledge DG, Parnell AC (2012) Modelling the effects of sediment compaction on salt marsh reconstructions of recent sea-level rise. Earth and Planetary Science Letters 345: 180-193 doi DOI 10.1016/j.epsl.2012.06.045

Braithwaite CJR, Montaggioni LF, Camoin GF, Dalmasso H, Dullo W-C, Mangini A (2000) Origins and development of Holocene coral reefs: a revisited model based on reef boreholes in the Seychelles, Indian Ocean. International Journal of Earth Science 89: 431-445

Bronk Ramsey C (2009) Bayesian analysis of radiocarbon dates. Radiocarbon 51: 337-360

Cabioch G, Montaggioni LF, Faure G, Ribaud-Laurenti A (1999) Reef coralgal assemblages as recorders of paleobathymetry and sea level changes in the Indo-Pacific province. Quaternary Sci Rev 18: 1681-1695

Camoin GF, Colonna M, Montaggioni LF, Casanova J, Faure G, Thomassin BA (1997) Holocene sea level changes and reef development in the southwestern Indian Ocean. Coral Reefs 16: 247-259

Camoin GF, Montaggioni LF, Braithwaite CJR (2004) Late glacial and post glacial sea levels in the Western Indian Ocean. Mar Geol 206: 119-146

Carlson AE, Legrande AN, Oppo DW, Came RE, Schmidt GA, Anslow FS, Licciardi JM, Obbink EA (2008) Rapid early Holocene deglaciation of the Laurentide ice sheet. Nature Geoscience 1: 620-624 doi Doi 10.1038/Ngeo285

Chappell J, Polach H (1991) Postglacial Sea-Level Rise from a Coral Record at Huon Peninsula, Papua-New-Guinea. Nature 349: 147-149

Church JA, White NJ, Hunter JR (2006) Sea-level rise at tropical Pacific and Indian Ocean islands. Global Planet Change 53: 155-168 doi DOI 10.1016/j.gloplacha.2006.04.001

Clark JA, Farrell WE, Peltier WR (1978) Global changes in post glacial sea-level: a numerical equation. Quaternary Res 9: 265-287

Conway H, Hall BL, Denton GH, Gades AM, Waddington ED (1999) Past and future grounding-line retreat of the West Antarctic Ice Sheet. Science 286: 280-283

Deschamps P, Durand N, Bard E, Hamelin B, Camoin G, Thomas AL, Henderson GM, Okuno J, Yokoyama Y (2012) Ice-sheet collapse and sea-level rise at the Bolling warming 14,600 years ago. Nature 483: 559-564 doi Doi 10.1038/Nature10902

Dziewonski AM, Anderson DL (1981) Preliminary Reference Earth Model. Phys Earth Planet In 25: 297-356 doi Doi 10.1016/0031-9201(81)90046-7

Edwards RL, Chen JH, Wasserburg GJ (1987) U-238 U-234-Th-230-Th-232 Systematics and the Precise Measurement of Time over the Past 500000 Years. Earth Planet Sc Lett 81: 175-192

Engelhart SE, Horton BP, Roberts DH, Bryant CL, Corbett DR (2007) Mangrove pollen of Indonesia and its suitability as a sea-level indicator. Mar Geol 242: 65-81 doi DOI 10.1016/j.margeo.2007.02.020

Fleming K, Johnston P, Zwartz D, Yokoyama Y, Lambeck K, Chappell J (1998) Refining the eustatic sea-level curve since the Last Glacial Maximum using far- and intermediate-field sites. Earth Planet Sc Lett 163: 327-342

Gehrels WR, Marshall WA, Gehrels MJ, Larsen G, Kirby JR, Eriksson J, Heinemeier J, Shimmield T (2006) Rapid sea-level rise in the North Atlantic Ocean since the first half of the 19th century. The Holocene 16: 948-964

Glasser NF, Harrison S, Winchester V, Aniya M (2004) Late Pleistocene and Holocene palaeoclimate and glacier fluctuations in Patagonia. Global Planet Change 43: 79-101 doi DOI 10.1016/j.gloplacha.2004.03.002

Glasser NF, Jansson KN, Harrison S, Rivera A (2005) Geomorphological evidence for variations of the North Patagonian Icefield during the Holocene. Geomorphology 71: 263-277 doi DOI 10.1016/j.geomorph.2005.02.003

Hanebuth T, Stattegger K, Grootes PM (2000) Rapid flooding of the Sunda Shelf: A late-glacial sea-level record. Science 288: 1033-1035

Hodgson DA, Bentley MJ (2013) Lake highstands in the Pensacola Mountains and Shackleton Range 4300-2250 cal. yr BP: Evidence of a warm climate anomaly in the interior of Antarctica. Holocene 23: 388-397 doi Doi 10.1177/0959683612460790

Hogg AG, Hua Q, Blackwell PG, Niu M, Buck CE, Guilderson TP, Heaton TJ, Palmer JG, Reimer PJ, Reimer RW, Turney CSM, Zimmerman SRH, (2013). . Radiocarbon (2013) SHCal13 Southern Hemisphere Calibration, 0-50,000 Years cal BP. Radiocarbon 55: 1889-1903

Horton B, Shennan I (2009) Compaction of Holocene strata and the implications for relative sea-level change on the east coast of England. Geology 37: 1083-1086 doi 10.1130/G30042A.1

Israelson C, Wohlfarth B (1999) Timing of the last-interglacial high sea level on the Seychelles Islands, Indian ocean. Quaternary Research 51: 306-316 doi DOI 10.1006/qres.1998.2030

Jackson LE, Barrie JV, Forbes DL, Shaw J, Manson GK, Schmidt M (2005) Effects of the 26 December 2004 Indian Ocean tsunami in the Republic of Seychelles.

Kelly M (1980) The status of the Neoglacial in Western Greenland. Rapport Grønlands Geologiske Undersøgelse 96: 1-24

Kemp A, Horton B, Culver S, Corbett D, van de Plassche O, Gehrels W, Douglas B, Parnell A (2009) Timing and magnitude of recent accelerated sea-level rise (North Carolina, United States). Geology 37: 1035-1038 doi 10.1130/G30352A.1

Kendall RA, Mitrovica JX, Milne GA (2005) On post-glacial sea level - II. Numerical formulation and comparative results on spherically symmetric models. Geophysical Journal International 161: 679-706 doi DOI 10.1111/j.1365-246X.2005.02553.x

Kennedy DM, Woodroffe CD (2002) Fringing reef growth and morphology: a review. Earth-Sci Rev 57: 255-277

Konrad SK, Clark DH (1998) Evidence for an early Neoglaciol glacier advance from rock glaciers Rind Lake sediments in the Sierra Nevada, California, USA. Arctic Alpine Res 30: 272-284 doi Doi 10.2307/1551975

Lambeck K (2002) Sea level change from mid Holocene to recent time: an Australian example with global implications. In: Mitrovica JX, Vermeersen BLA (eds) Ice Sheets, Sea Level and the Dynamic Earth, Geodynamics Series 29. American Geophysical Union, pp 33-50

Lambeck K, Anzidei M, Antonioli F, Benini A, Esposito A (2004) Sea level in Roman time in the Central Mediterranean and implications for recent change. Earth Planet Sc Lett 224: 563-575

Lambeck K, Purcell A (2005) Sea-level change in the Mediterranean Sea since the LGM: Model predictions for tectonically stable areas. Quaternary Sci Rev 24: 1969-1988

Lambeck K, Rouby H, Purcell A, Sun Y, Sambridge M (2014) Sea level and global ice volumes from the Last Glacial Maximum to the Holocene. P Natl Acad Sci USA 111: 15296-15303

Lecavalier B, Milne GA, Simpson MJR, Wake LM, Huybrechts P, Tarasov L, Kjeldsen KK, Funder SV, Long AJ, Woodroffe SA, Dyke A, Larsen NK (2014) A model of Greenland ice sheet deglaciation based on observations of relative sea-level and ice extent. Quaternary Sci Rev in press

Lewis MS (1969) Sedimentary Environments and Unconsolidated Carbonate Sediments of Fringing Coral Reefs of Mahe, Seychelles. Mar Geol 7: 95-127

Li C, Li Y, Burr GS (2014) Testing the accuracy of ^{14}C age data from pollen concentrates in the Yangtze delta, China. Radiocarbon 56: 1-7

Ludwig KR (1991) ISOPLOT—a plotting and regression program for radiogenic-isotope data. USGS Open-File Report: 91-445

Marcott SA, Shakun JD, Clark PU, Mix AC (2013) A Reconstruction of Regional and Global Temperature for the Past 11,300 Years. Science 339: 1198-1201 doi DOI 10.1126/science.1228026

Mason AJ, Henderson GM (2010) Correction of multi-collector-ICP-MS instrumental biases in high-precision uranium-thorium chronology. Int J Mass Spectrom 295: 26-35 doi DOI 10.1016/j.ijms.2010.06.016

Milne G, Mitrovica JX (2008) Searching for eustasy in deglacial sea-level histories. Quaternary Sci Rev 27: 2292-2302

Milne G, Peros M (2013) Data-model comparison of Holocene sea-level change in the circum-Caribbean region. Global and Planetary Change 107: 119-131 doi 10.1016/j.gloplacha.2013.04.014

Milne GA, Long AJ, Bassett SE (2005) Modelling Holocene relative sea-level observations from the Caribbean and South America. Quaternary Sci Rev 24: 1183-1202

Milne GA, Mitrovica JX (1998) The influence of time-dependent ocean-continent geometry on predictions of post-glacial sea level change in Australia and New Zealand. Geophys Res Lett 25: 793-796 doi Doi 10.1029/98gl00498

Mitrovica JX, Milne GA (2002) On the origin of late Holocene sea-level highstands within equatorial ocean basins. Quaternary Sci Rev 21: 2179-2190

Mitrovica JX, Milne GA (2003) On post-glacial sea level: I. General theory. Geophysical Journal International 154: 253-267 doi DOI 10.1046/j.1365-246X.2003.01942.x

Mitrovica JX, Peltier WR (1991) On Postglacial Geoid Subsidence over the Equatorial Oceans. Journal of Geophysical Research-Solid Earth 96: 20053-20071

Mitrovica JX, Wahr J, Matsuyama I, Paulson A (2005) The rotational stability of an ice-age earth. Geophysical Journal International 161: 491-506 doi DOI 10.1111/j.1365-246X.2005.02609.x

Montaggioni LF, Faure G (1997) Response of reef coral communities to sea-level rise: a Holocene model from Mauritius (Western Indian Ocean). Sedimentology 44: 1053-1070

Nakada M, Lambeck K (1988) The Melting History of the Late Pleistocene Antarctic Ice-Sheet. Nature 333: 36-40 doi Doi 10.1038/333036a0

Nakada M, Lambeck K (1989) Late Pleistocene and Holocene Sea-Level Change in the Australian Region and Mantle Rheology. Geophysical Journal-Oxford 96: 497-517

Newnham RM, Vandergoes MJ, Garnett MH, Lowe DJ, Prior C, Almond PC (2007) Test of AMS C-14 dating of pollen concentrates using tephrochronology. Journal of Quaternary Science 22: 37-51 doi Doi 10.1002/Jqs.1016

Peltier WR (2002) On eustatic sea level history: Last Glacial Maximum to Holocene. Quaternary Sci Rev 21: 377-396

Peltier WR (2004) Global glacial isostasy and the surface of the ice-age earth: The ICE-5G (VM2) model and GRACE. Annual Review of Earth and Planetary Sciences 32: 111-149 doi 10.1146/annurev.earth.32.082503.144359

Peltier WR, Fairbanks RG (2006) Global glacial ice volume and Last Glacial Maximum duration from an extended Barbados sea level record. Quaternary Sci Rev 25: 3322-3337

Pirazzoli PA, Kaplin PA, Montaggioni LF (1990) Differential Vertical Crustal Movements Deduced from Late Holocene Coral-Rich Conglomerates - Farquhar and St-Joseph Atolls (Seychelles, Western Indian-Ocean). J Coastal Res 6: 381-389

Reimer PJ, Bard E, Bayliss A, Beck JW, Blackwell PG, Ramsey CB, Buck CE, Cheng H, Edwards RL, Friedrich M, Grootes PM, Guilderson TP, Haflidason H, Hajdas I, Hatte C, Heaton TJ, Hoffmann DL, Hogg AG, Hughen KA, Kaiser KF, Kromer B, Manning SW, Niu M, Reimer RW, Richards DA, Scott EM, Southon JR, Staff RA, Turney CSM, van der Plicht J (2013) Intcal13 and Marine13 Radiocarbon Age Calibration Curves 0-50,000 Years Cal Bp. Radiocarbon 55: 1869-1887

Schofield JC (1977) Late Holocene Sea-Level, Gilbert and Ellice Islands, West Central Pacific Ocean. New Zeal J Geol Geop 20: 503-529

Simpson MJR, Milne GA, Huybrechts P, Long AJ (2009) Calibrating a glaciological model of the Greenland ice sheet from the last glacial maximum to present-day using field observations of relative sea level and ice extent. Quaternary Sci Rev 28: 1631-1657

Sivan D, Lambeck K, Toueg R, Raban A, Porath Y, Shirman B (2004) Ancient coastal wells of Caesarea Maritima, Israel, an indicator for relative sea level changes during the last 2000 years. Earth Planet Sc Lett 222: 315-330 doi DOI 10.1016/j.epsl.2004.02.007

Sivan D, Schattner U, Morhange C, Boaretto E (2010) What can a sessile mollusk tell about neotectonics? Earth Planet Sc Lett 296: 451-458 doi DOI 10.1016/j.epsl.2010.05.032

Smith WG, Coleman JM (1967) Recent Submergence of Southern Florida - Discussion. Geol Soc Am Bull 78: 1191-& doi Doi 10.1130/0016-7606(1967)78[1191:Rsosfd]2.0.Co;2

Southon J, Kashgarian M, Fontugne M, Metivier B, Yim WWS (2002) Marine reservoir corrections for the Indian Ocean and southeast Asia. Radiocarbon 44: 167-180

Sterken M, Roberts SJ, Hodgson DA, Vyverman W, Balbo AL, Sabbe K, Moreton SG, Verleyen E (2012) Holocene glacial and climate history of Prince Gustav Channel, northeastern Antarctic Peninsula. Quaternary Sci Rev 31: 93-111 doi DOI 10.1016/j.quascirev.2011.10.017

Stone JO, Balco GA, Sugden DE, Caffee MW, Sass LC, Cowdery SG, Siddoway C (2003) Holocene deglaciation of Marie Byrd Land, West Antarctica. Science 299: 99-102 doi DOI 10.1126/science.1077998

Toker E, Sivan D, Stern E, Shirman B, Tsimplis M, Spada G (2012) Evidence for centennial scale sea level variability during the Medieval Climate Optimum (Crusader Period) in Israel, eastern Mediterranean. Earth Planet Sc Lett 315: 51-61 doi DOI 10.1016/j.epsl.2011.07.019

Tornqvist T, Wallace D, Storms J, Wallinga J, Van Dam R, Blaauw M, Derksen M, Klerks C, Meijneken C, Snijders E (2008) Mississippi Delta subsidence primarily caused by compaction of Holocene strata. Nature Geoscience 1: 173-176 doi 10.1038/ngeo129

Torsvik TH, Ashwal LD, Tucker RD, Eide EA (2001) Neoproterozoic geochronology and palaeogeography of the Seychelles microcontinent: the India link. Precambrian Res 110: 47-59

Vandergoes MJ, Prior CA (2003) AMS dating of pollen concentrates-a methodological study of late Quaternary sediments from south westland, New Zealand. Radiocarbon 45: 479-491

Whitehouse PL, Bentley MJ, Milne GA, King MA, Thomas ID (2012) A new glacial isostatic adjustment model for Antarctica: calibrated and tested using observations of relative sea-level change and present-

day uplift rates. Geophysical Journal International 190: 1464-1482 doi DOI 10.1111/j.1365-246X.2012.05557.x

Whitehouse PL, Bradley SL (2013) Eustatic sea-level changes since the Last Glacial Maximum. In: Elias SA (ed) Encyclopedia of Quaternary Science. Elsevier, Amsterdam, pp 439-451

Woodroffe CD (1981) Mangrove Swamp Stratigraphy and Holocene Transgression, Grand Cayman Island, West-Indies. Mar Geol 41: 271-294 doi Doi 10.1016/0025-3227(81)90085-2

Woodroffe CD (1988a) Changing mangrove and wetland environments over the last 8000 years, northern Australia and southeast Asia. In: Wade-Marshall D, Loveday P (eds) Northern Australia: Progress and Propects Volume 2: Floodplains Research, North Australia Research Unit, Australian National University, Canberra, pp 1-33

Woodroffe CD (1988b) Mangroves and sedimentation in reef environments: indicators of past sea-level changes, and present sea-level trends? . Proceedings of the 6th International Coral Reef Congress: 535-539

Woodroffe CD (1990) The Impact of Sea-Level Rise on Mangrove Shorelines. Prog Phys Geog 14: 483-520 doi Doi 10.1177/030913339001400404

Woodroffe CD, McGregor HV, Lambeck K, Smithers SG, Fink D (2012) Mid-Pacific microatolls record sea-level stability over the past 5000 yr. Geology 40: 951-954

Woodroffe CD, Thom BG, Chappell J (1985) Development of Widespread Mangrove Swamps in Mid-Holocene Times in Northern Australia. Nature 317: 711-713 doi Doi 10.1038/317711a0

Woodroffe SA, Horton BP, Larcombe P, Whittaker JE (2005) Contemporary intertidal foraminifera distributions of mangrove environments from the central Great Barrier Reef shelf, Australia: implications for sea-level reconstructions. Journal of Foraminiferal Research 35: 259-270

Woodroffe SA, Long AJ, Punwong P, Selby K, Bryant CL, Marchant R (2015) Radiocarbon dating of mangrove sediments to constrain Holocene sea-level change on Zanzibar in the Southwest Indian Ocean. Holocene 25: 820-831.

Yokoyama Y, Lambeck K, De Deckker P, Johnston P, Fifield IK (2000) Timing of the Last Glacial Maximum from observed sea-level minima. Nature 406: 713-716

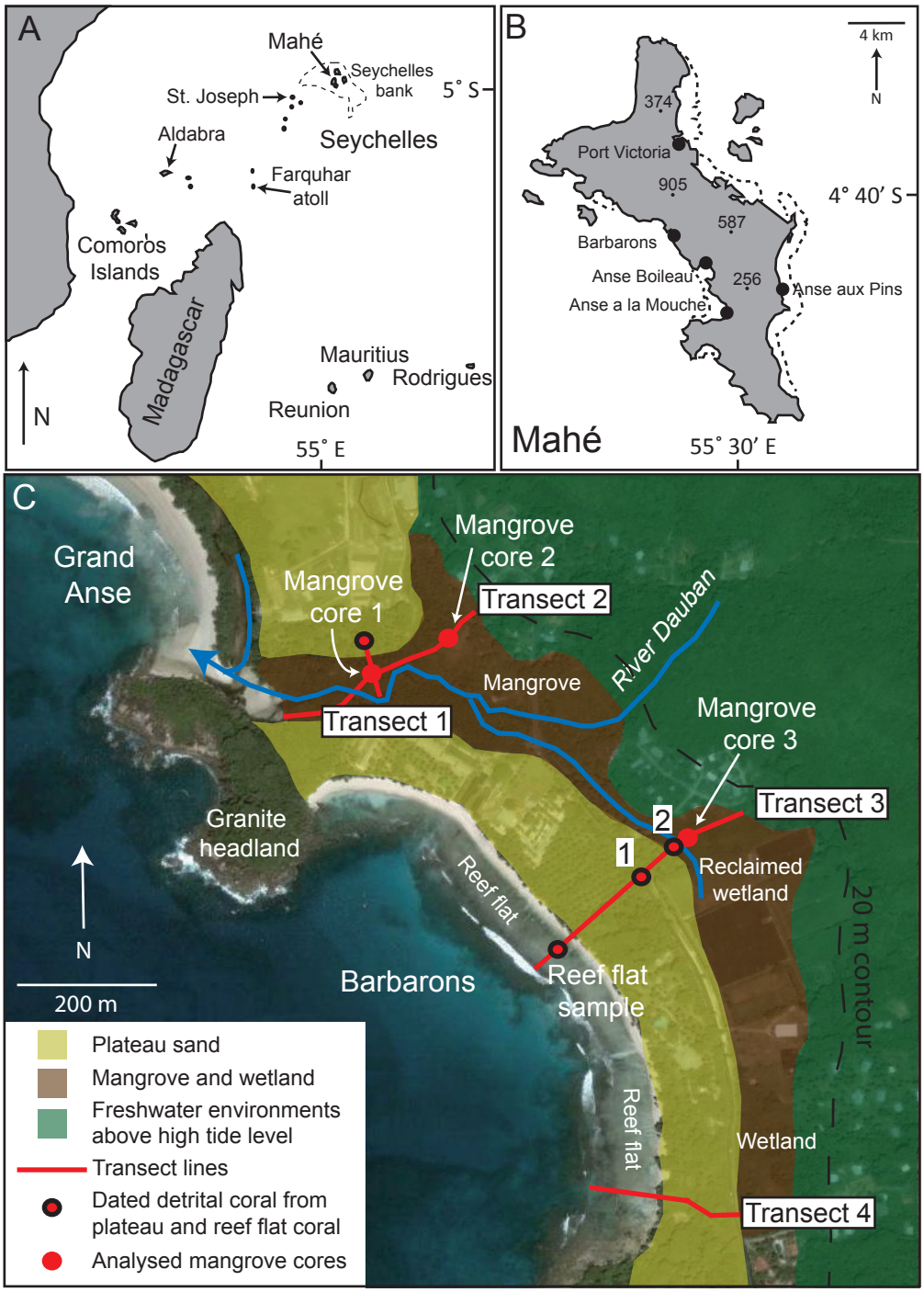
A
Mahé
Seychelles bank
St. Joseph
5° S
Aldabra
Seychelles
Farquhar atoll
Comoros Islands
Madagascar
Mauritius
Rodrigues
Reunion
N
55° E
B
4 km
N
374
Port Victoria
905
4° 40′ S
587
Barbarons
Anse Boileau
256
Anse aux Pins
Anse a la Mouche
Mahé
55° 30′ E
C
Grand Anse
Mangrove core 2
Mangrove core 1
Transect 2
River Dauban
Mangrove
Transect 1
Mangrove core 3
Transect 3
Granite headland
2
1
Reclaimed wetland
Reef flat
20 m contour
N
200 m
Barbarons
Reef flat sample
Reef flat
Wetland
Transect 4
Plateau sand
Mangrove and wetland
Freshwater environments above high tide level
Transect lines
Dated detrital coral from plateau and reef flat coral
Analysed mangrove cores

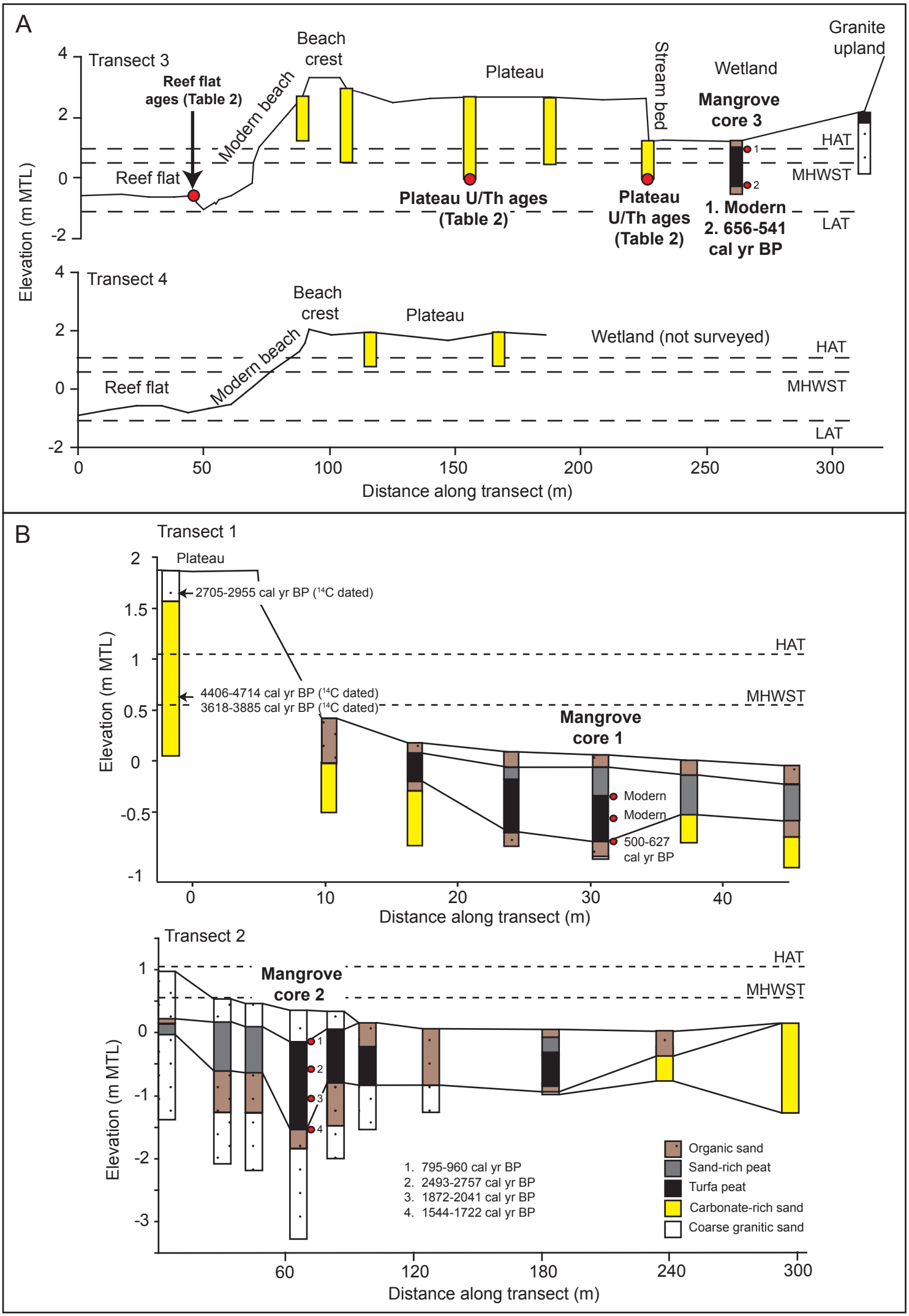
A
Transect 3
Reef flat ages (Table 2)
Reef flat
Modern beach
Beach crest
Plateau
Stream bed
Wetland
Mangrove core 3
Granite upland
HAT
MHWST
LAT
Plateau U/Th ages (Table 2)
Plateau U/Th ages (Table 2)
1. Modern
2. 656-541 cal yr BP
Transect 4
Beach crest
Plateau
Wetland (not surveyed)
Modern beach
Reef flat
Elevation (m MTL)
Distance along transect (m)
B
Transect 1
Plateau
2705-2955 cal yr BP (14C dated)
4406-4714 cal yr BP (14C dated)
3618-3885 cal yr BP (14C dated)
Mangrove core 1
Modern
Modern
500-627 cal yr BP
Transect 2
Mangrove core 2
1. 795-960 cal yr BP
2. 2493-2757 cal yr BP
3. 1872-2041 cal yr BP
4. 1544-1722 cal yr BP
Organic sand
Sand-rich peat
Turfa peat
Carbonate-rich sand
Coarse granitic sand

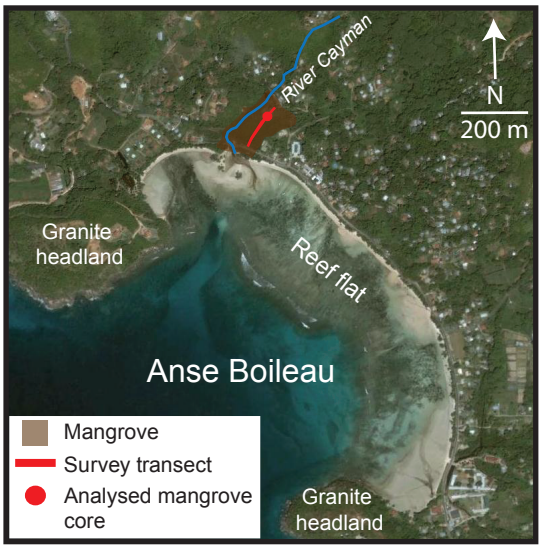
River Cayman
N
200 m
Granite headland
Reef flat
Anse Boileau
Mangrove
Survey transect
Analysed mangrove core
Granite headland

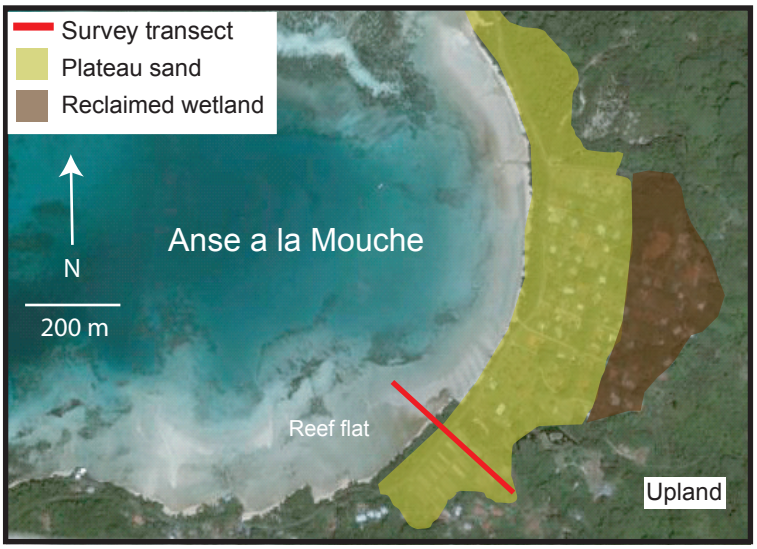
Survey transect
Plateau sand
Reclaimed wetland
N
200 m
Anse a la Mouche
Reef flat
Upland

A

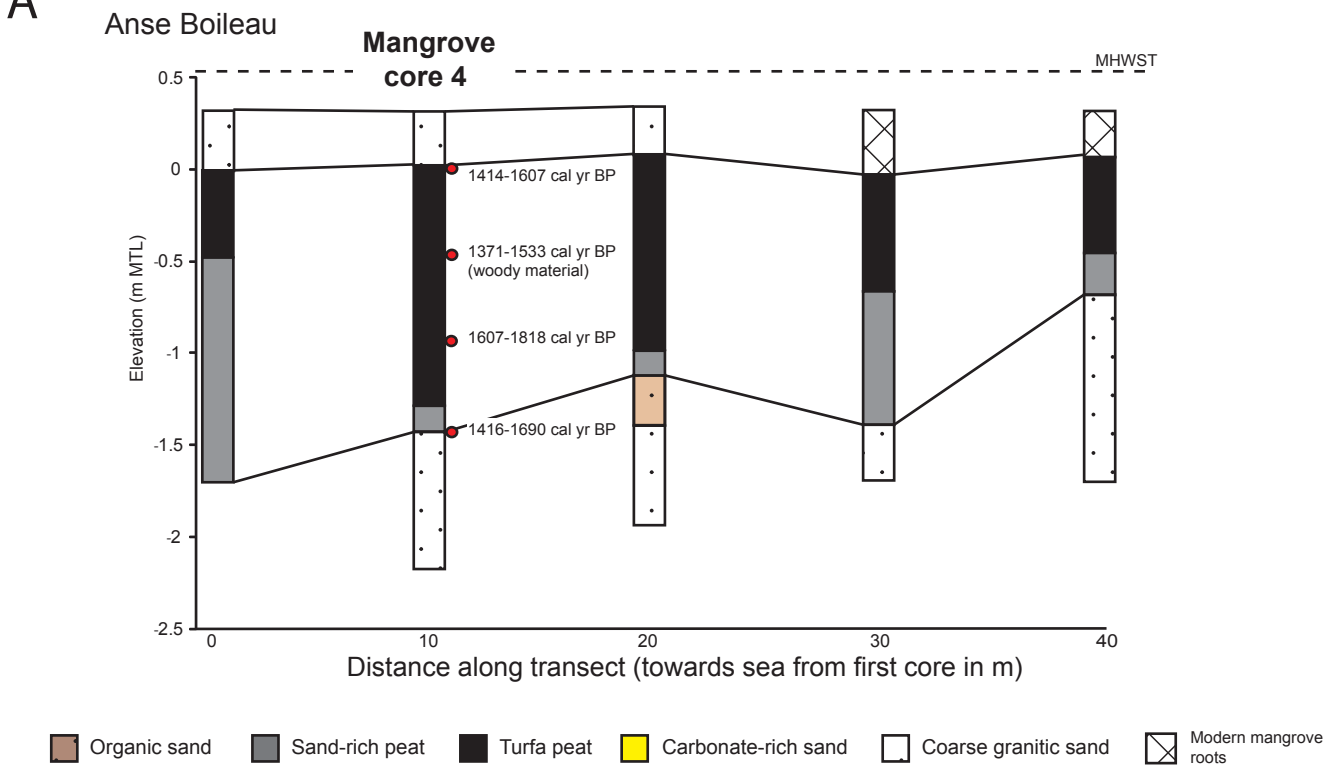
Anse Boileau
Mangrove core 4
MHWST
0.5
0
-0.5
-1
-1.5
-2
-2.5
Elevation (m MTL)
1414-1607 cal yr BP
1371-1533 cal yr BP (woody material)
1607-1818 cal yr BP
1416-1690 cal yr BP
0
10
20
30
40
Distance along transect (towards sea from first core in m)
Organic sand
Sand-rich peat
Turfa peat
Carbonate-rich sand
Coarse granitic sand
Modern mangrove roots

B

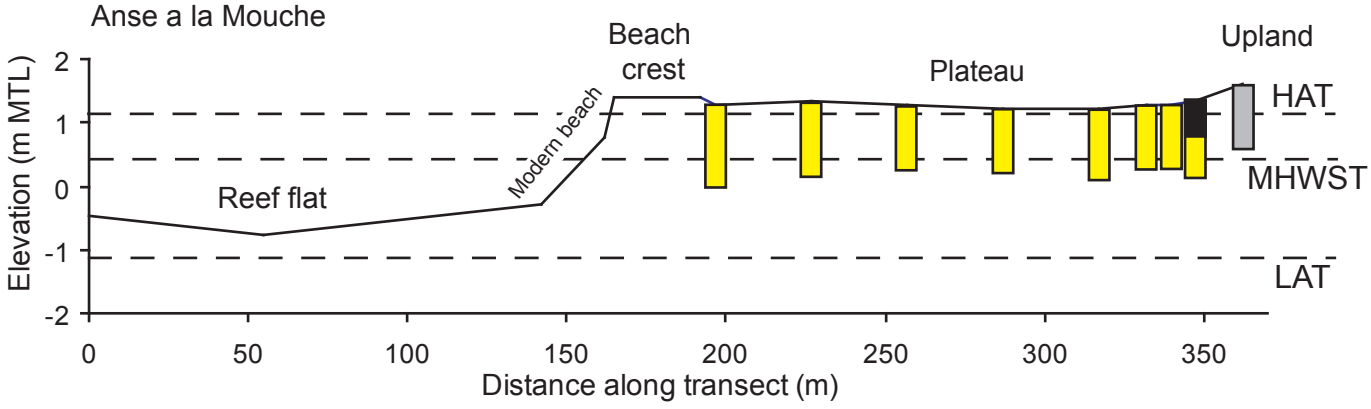
Anse a la Mouche
Beach crest
Plateau
Upland
HAT
MHWST
LAT
Modern beach
Reef flat
Elevation (m MTL)
2
1
0
-1
-2
0
50
100
150
200
250
300
350
Distance along transect (m)

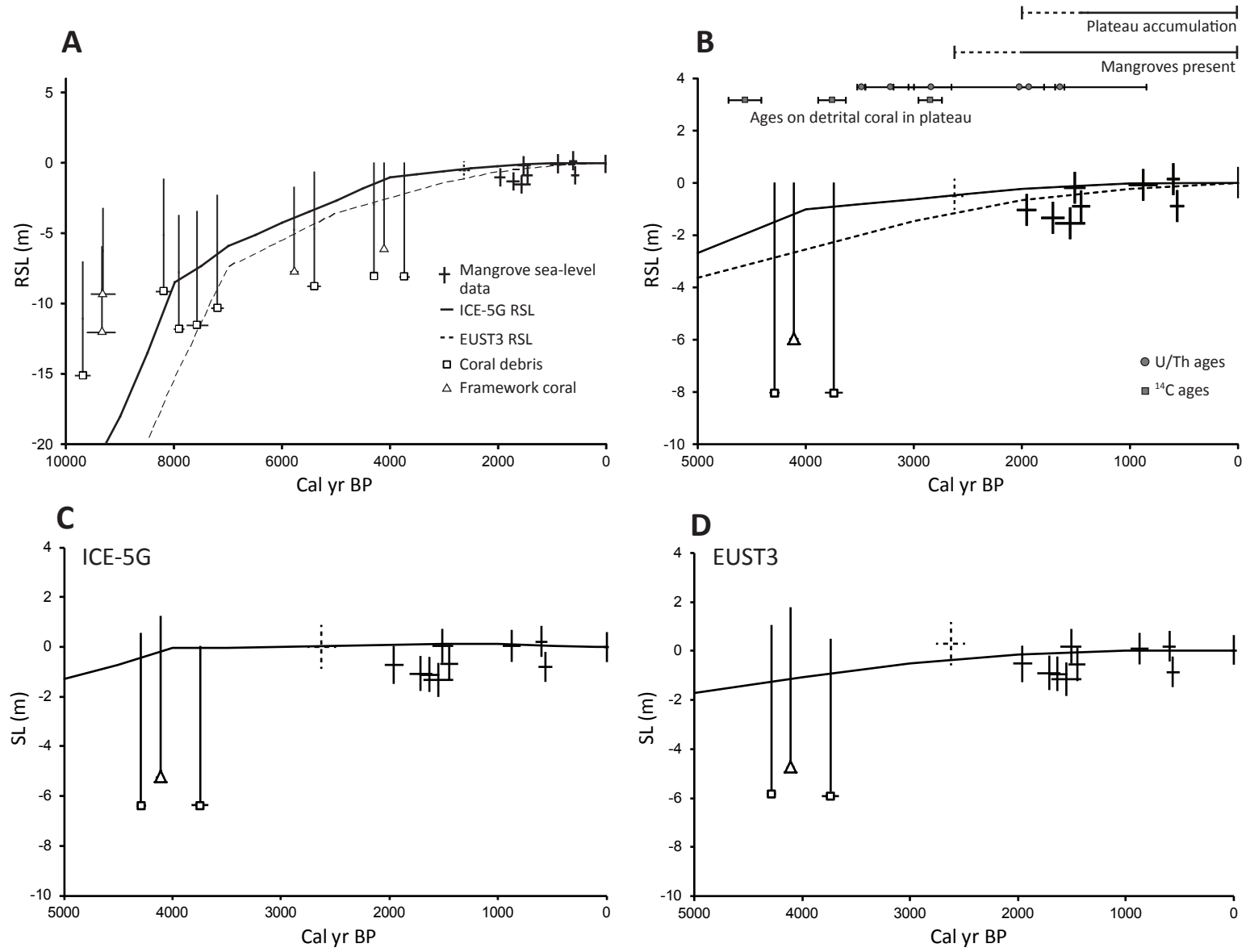
A
RSL (m)
Cal yr BP
Mangrove sea-level data
ICE-5G RSL
EUST3 RSL
Coral debris
Framework coral
B
Plateau accumulation
Mangroves present
Ages on detrital coral in plateau
U/Th ages
14C ages
RSL (m)
Cal yr BP
C
ICE-5G
SL (m)
Cal yr BP
D
EUST3
SL (m)
Cal yr BP

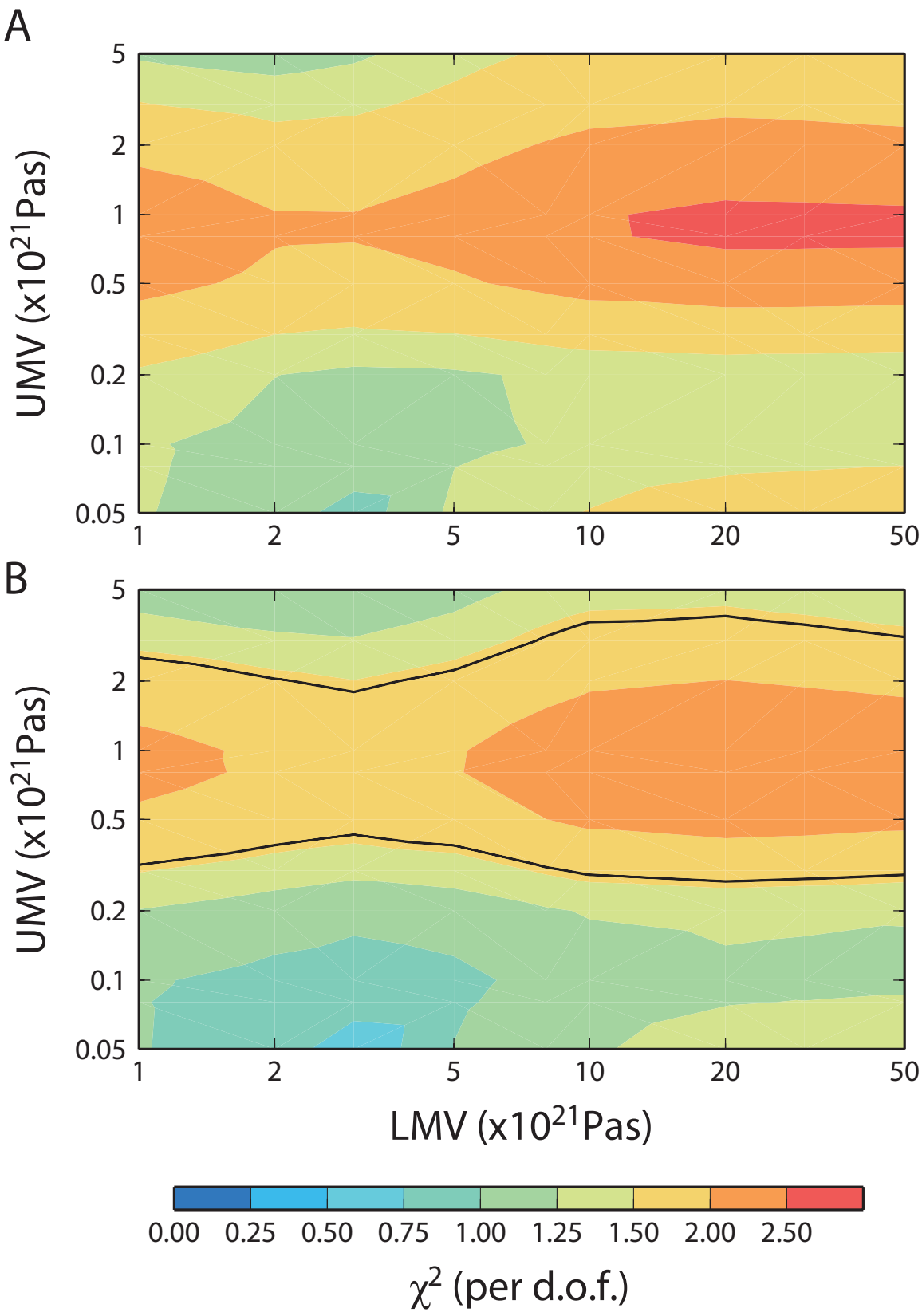
A
B
UMV (x10^21Pas)
5
2
1
0.5
0.2
0.1
0.05
1
2
5
10
20
50
LMV (x10^21Pas)
0.00
0.25
0.50
0.75
1.00
1.25
1.50
2.00
2.50
χ2 (per d.o.f.)

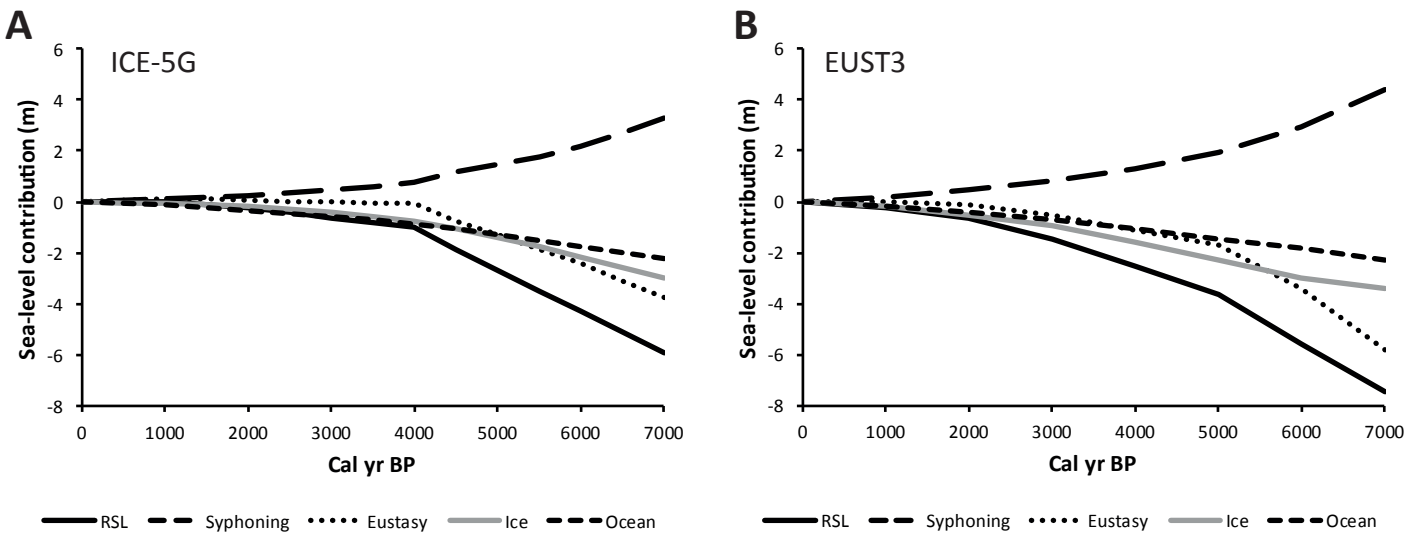
A
ICE-5G
Sea-level contribution (m)
6
4
2
0
-2
-4
-6
-8
0
1000
2000
3000
4000
5000
6000
7000
Cal yr BP
RSL
Syphoning
Eustasy
Ice
Ocean
B
EUST3
Sea-level contribution (m)
Cal yr BP
RSL
Syphoning
Eustasy
Ice
Ocean

Mangrove material from Barbarons and Anse Boileau	**Depth in core (m)**	**Elevation (m MTL)**	**Laboratory code**	**^{14}C age (± 1 σ)**	**Maximum age (cal yr BP, 2σ)**	**Minimum age (cal yr BP, 2σ)**	**Indicative meaning (m MTL)**	**RSL (m MTL)**
Barbarons Transect 1 Mangrove core 1	0.28	-0.16	SUERC-29503	Modern	n/a	n/a	Limiting	At present
	0.53	-0.41	SUERC-29506	Modern	n/a	n/a	Limiting	At present
	0.53*	-0.41	SUERC-31712	Modern	n/a	n/a	n/a	Not used
	0.80	-0.68	SUERC-29507	504 ± 37	627	500	0.20 ± 0.6	-0.88 ± 0.6
Barbarons Transect 2 Mangrove core 2	0.32	0.13	SUERC-29500	983 ± 37	960	795	0.20 ± 0.6	-0.07 ± 0.6
	0.32*	0.13	SUERC-31709	969 ± 37			n/a	Not used
	0.75	-0.3	SUERC-30458	2559 ± 37	2757	2493	0.20 ± 0.6	-0.50 ± 0.6
	1.28	-0.83	SUERC-29501	1998 ± 37	2041	1872	0.20 ± 0.6	-1.03 ± 0.6
	1.61	-1.16	SUERC-29502	1733 ± 37	1722	1544	0.20 ± 0.6	-1.36 ± 0.6
Barbarons Transect 3 Mangrove core 3	0.31	0.88	SUERC-37542	Modern	n/a	n/a	Limiting	At present
	0.84	0.35	SUERC-37543	602 ± 27	656	541	0.20 ± 0.6	0.14 ± 0.6
Anse Boileau Mangrove core 4	0.29	0.02	SUERC-29508	1630 ± 35	1607	1414	0.20 ± 0.6	-0.18 ± 0.6
	1.00 (bulk sediment)	-0.69	SUERC-29509	Modern	n/a	n/a	0.20 ± 0.6	Not used
	1.00 (fine root hairs)	-0.69	SUERC-32436	983 ± 37	960	795	0.20 ± 0.6	Not used
	1.00 (woody material)	-0.69	SUERC-32437	1559 ± 37	1533	1371	0.20 ± 0.6	-0.89 ± 0.6
	1.44	-1.13	SUERC-29510	1779 ± 35	1818	1607	0.20 ± 0.6	-1.33 ± 0.6
	1.65	-1.34	SUERC-29511	1650 ± 37	1690	1416	0.20 ± 0.6	-1.54 ± 0.6
Detrital coral from plateaux at Barbarons	**Depth in core (m)**	**ΔR value**	**Laboratory code**	**^{14}C age (± 1 σ)**	**Maximum age (cal yr BP, 2σ)**	**Minimum age (cal yr BP, 2σ)**		
Barbarons Transect 1	0.60	140 ± 25	SUERC-28868	3212 ± 37	2957	2739		
Barbarons Transect 1	1.70	140 ± 25	SUERC-32441	3953 ± 37	3885	3629		
Barbarons Transect 1	1.70	140 ± 25	SUERC-28867	4539 ±35	4715	4411		

Sample	Depth in core (m)	^{238}U ppm	Error (2 σ)	^{232}Th ppm	Error (2 σ)	$^{232}Th/^{238}U$	Error (2 σ)	$^{230}Th/^{238}U$	Error (2 σ)	$^{234}U/^{238}U$	Error (2 σ)	Age Cal yr BP ± 2 σ	$(^{234}U/^{238}U)_0$	Error (2 σ)
Barbarons Transect 3 Core 1	1.35	4.408	0.008	350	2	0.02602	0.00013	0.04271	0.00025	1.1447	0.0009	2000 ± 1200	1.149	0.006
Barbarons Transect 3 Core 1	1.45	3.852	0.01	59.76	0.29	0.005079	0.000028	0.03808	0.00017	1.1466	0.0009	3220 ± 230	1.1486	0.0014
Barbarons Transect 3 Core 1	1.45	3.865	0.008	52.96	0.21	0.004487	0.000020	0.03380	0.00016	1.1464	0.0009	2850 ± 200	1.1482	0.0013
Barbarons Transect 3 Core 2	0.80	4.184	0.005	33.90	0.13	0.002653	0.000010	0.02270	0.00011	1.1461	0.0009	1910 ± 120	1.1472	0.0011
Barbarons Transect 3 Core 2	0.80	2.7441	0.0019	5.288	0.024	0.000631	0.000003	0.03720	0.00023	1.1470	0.0014	3490 ± 40	1.1486	0.0014
Barbarons Transect 3 Core 2	0.83	5.54	0.04	14.92	0.06	0.000881	0.000007	0.01857	0.00016	1.1475	0.0009	1650 ± 40	1.1483	0.0009
Reef flat sample 1	n/a	0.4475	0.0005	10.85	0.05	0.00794	0.00004	0.0383	0.0007	1.1470	0.0014	3000 ± 400	1.1493	0.0023
Reef flat sample 2	n/a	2.858	0.006	0.615	0.007	0.000070	0.000001	0.00124	0.00006	1.1477	0.0014	50 ± 7	1.1478	0.0014
Reef flat sample 3	n/a	0.8324	0.001	40.67	0.20	0.01600	0.00008	0.0720	0.0007	1.1458	0.0014	5800 ± 700	1.150	0.004
Assumed detrital component						1.21	± 0.605	1	± 0.25	1	± 0.25			

Mangrove data (new this study)	Depth in core (m)	Elevation (m MTL)	Maximum age (cal yr BP, 2σ)	Minimum age (cal yr BP, 2σ)	Indicative meaning (m MTL)	RSL (m MTL)	Optimal earth model GIA correction ICE-5G (m)	Optimal earth model GIA correction EUST3 (m)	Eustatic SL ICE-5G (m MTL)	Eustatic SL EUST3 (m MTL)
Barbarons Mangrove core 1	0.80	-0.68	627	500	0.20 ± 0.60	-0.88 ± 0.60	-0.07 ± 0.11	-0.04 ± 0.10	-0.82 ± 0.61	-0.82 ± 0.61
Barbarons Mangrove core 2	0.32	0.13	960	795	0.20 ± 0.60	-0.07 ± 0.60	-0.11 ± 0.19	-0.17 ± 0.18	0.04 ± 0.63	0.10 ± 0.63
	0.75	-0.3	2757	2493	0.20 ± 0.60	-0.50 ± 0.60	-0.49 ± 0.65	-0.79 ± 0.65	-0.02 ± 0.88	0.29 ± 0.89
	1.28	-0.83	2041	1872	0.20 ± 0.60	-1.03 ± 0.60	-0.31 ± 0.45	-0.52 ± 0.45	-0.73 ± 0.75	-0.51 ± 0.75
	1.61	-1.16	1722	1544	0.20 ± 0.60	-1.36 ± 0.60	-0.24 ± 0.36	-0.42 ± 0.37	-1.12 ± 0.70	-0.94 ± 0.70
Barbarons Mangrove core 3	0.31	0.88	Modern	Modern	Limiting	At present	0	0	0	0
	0.84	0.35	656	541	0.20 ± 0.60	0.14 ± 0.60	-0.07 ± 0.12	-0.05 ± 0.11	0.22 ± 0.61	0.20 ± 0.61
Anse Boileau Mangrove core 4	0.29	0.02	1607	1414	0.20 ± 0.60	-0.18 ± 0.60	-0.22 ± 0.33	-0.39 ± 0.34	0.03 ± 0.69	0.20 ± 0.69
	1.00 (woody material)	-0.69	1533	1371	0.20 ± 0.60	-0.89 ± 0.60	-0.21 ± 0.32	-0.37 ± 0.32	-0.69 ± 0.68	-0.53 ± 0.68
	1.44	-1.13	1818	1607	0.20 ± 0.60	-1.33 ± 0.60	-0.26 ± 0.39	-0.45 ± 0.39	-1.08 ± 0.71	-0.89 ± 0.71
	1.65	-1.34	1690	1416	0.20 ± 0.60	-1.54 ± 0.60	-0.23 ± 0.34	-0.40 ± 0.35	-1.32 ± 0.69	-1.15 ± 0.69
Coral data (Braithwaite et al., 2000)	**Depth below reef flat (m)**	**Elevation (m MTL)**	**Maximum age ($^{234}U/^{238}U$)**	**Minimum age ($^{234}U/^{238}U$)**	**Indicative meaning (m MTL)**	**RSL (m MTL)**	**Optimal earth model GIA correction ICE-5G (m)**	**Optimal earth model GIA correction EUST3 (m)**	**Eustatic SL ICE-5G (m MTL)**	**Eustatic SL EUST3 (m MTL)**
Coral debris AP4	-1.80	-2.51	3820	3660	-4.71 ± 4	-4.00 ± 4	-0.87 ± 1.05	-1.33 ± 1.09	-3.13 ± 3.18	-2.67 ± 3.19
Coral debris	-4.40	-5.11	4334	4244	-4.71 ± 4	-4.00 ± 4	-1.05 ± 1.81	-1.59 ± 1.79	-2.95 ± 3.50	-2.41 ± 3.49
Coral debris AP1	-8.70	-9.41	5510	5290	-4.71 ± 4	-4.70 ± 4	-1.59 ± 2.83	-2.02 ± 1.95	-3.11 ± 4.90	-2.68 ± 4.45
Coral debris AP4	-10.30	-11.01	7300	7100	-4.71 ± 4	-6.30 ± 4	-2.24 ± 2.97	-1.29 ± 2.04	-4.06 ± 4.98	-5.01 ± 4.49
Coral debris AP4	-11.50	-12.21	7765	7395	-4.71 ± 4	-7.50 ± 4	-2.31 ± 2.98	-0.67 ± 2.90	-5.19 ± 4.99	-6.83 ± 4.94
Coral debris AP4	-11.80	-12.51	7990	7830	-4.71 ± 4	-7.80 ± 4	-2.28 ± 1.19	-0.13 ± 1.25	-5.52 ± 4.17	-7.67 ± 4.19
Coral sands AP8	-9.15	-9.86	8330	8070	-4.71 ± 4	-5.15 ± 4	-1.87 ± 2.00	0.26 ± 1.92	-3.28 ± 4.47	-5.41 ± 4.44
Coral debris AP4	-15.10	-15.81	9830	9570	-4.71 ± 4	-11.1 ± 4	-0.43 ± 0.00	2.35 ± 0.00	-10.67 ± 4.00	-13.45 ± 4.00
Framework coral AP2	-4.20	-4.91	4150	4070	-3.71 ± 3	-3.00 ± 3	-0.99 ± 1.27	-1.51 ± 1.33	-2.00 ± 3.26	-1.49 ± 3.28
Framework coral AP8	-7.75	-8.46	5840	5700	-3.71 ± 3	-4.75 ± 3	-1.76 ± 2.92	-2.11 ± 1.94	-2.99 ± 4.18	-2.64 ± 3.57

Framework coral AP8	-9.30	-10.01	9550	9110	-3.71 ± 3	-6.30 ± 3	-0.63 ± 2.99	1.76 ± 2.70	-5.67 ± 4.23	-8.06 ± 4.04
Framework coral AP8	-12.00	-12.71	9600	9100	-3.71 ± 3	-9.00 ± 3	-0.62 ± 2.99	1.79 ± 2.71	-8.39 ± 4.23	-10.79 ± 4.04